and analyzed the data. M.T. provided intellectual support. M.Y., N.K., S.T., and A.S. provided clinical samples. H. Yotsuyanagi designed the experiments, analyzed the data and wrote the manuscript. K.K. provided intellectual support. F.I. supervised all aspects of the study.

References

Adey A, Burton JN, Kitzman JO, Hiatt JB, Lewis AP, Martin BK, Qiu R, Lee C, Shendure J. 2013. The haplotype-resolved genome and epigenome of the aneuploid HeLa cancer cell line. *Nature* **500:** 207–211.

Burgers WA, Blanchon L, Pradhan S, de Launoit Y, Kouzarides T, Fuks F. 2007. Viral oncoproteins target the DNA methyltransferases. *Oncogene* **26:** 1650–1655.

Cheung VG, Nowak N, Jang W, Kirsch IR, Zhao S, Chen XN, Furey TS, Kim UJ, Kuo WL, Olivier M, et al. 2001. Integration of cytogenetic landmarks into the draft sequence of the human genome. *Nature* **409:** 953–958.

Ding D, Lou X, Hua D, Yu W, Li L, Wang J, Gao F, Zhao N, Ren G, Li L, et al. 2012. Recurrent targeted genes of hepatitis B virus in the liver cancer genomes identified by a next-generation sequencing-based approach. *PLoS Genet* **8:** e1003065.

Doerfler W. 2008. In pursuit of the first recognized epigenetic signal-DNA methylation: a 1976 to 2008 synopsis. *Epigenetics* **3:** 125–133.

Doerfler W, Remus R, Müller K, Heller H, Hohlweg U, Schubbert R. 2001. The fate of foreign DNA in mammalian cells and organisms. *Dev Biol* **106:** 89–97.

Durbin R, Eddy S, Krogh A, Mitchison G. 1998. *Biological sequence analysis.* Cambridge University Press, Cambridge, UK.

Fernandez AF, Rosales C, Lopez-Nieva P, Graña O, Ballestar E, Ropero S, Espada J, Melo SA, Lujambio A, Fraga MF, et al. 2009. The dynamic DNA methylomes of double-stranded DNA viruses associated with human cancer. *Genome Res* **19:** 438–451.

Fujimoto A, Totoki Y, Abe T, Boroevich KA, Hosoda F, Nguyen HH, Aoki M, Hosono N, Kubo M, Miya F, et al. 2012. Whole-genome sequencing of liver cancers identifies etiological influences on mutation patterns and recurrent mutations in chromatin regulators. *Nat Genet* **44:** 760–764.

Furey TS, Haussler D. 2003. Integration of the cytogenetic map with the draft human genome sequence. *Hum Mol Genet* **12:** 1037–1044.

Gatza ML, Chandhasin C, Ducu RI, Marriott SJ. 2005. Impact of transforming viruses on cellular mutagenesis, genome stability, and cellular transformation. *Environ Mol Mutagen* **45:** 304–325.

Hilleman MR. 2004. Strategies and mechanisms for host and pathogen survival in acute and persistent viral infections. *Proc Natl Acad Sci* **101:** 14560–14566.

Igarashi S, Suzuki H, Niinuma T, Shimizu H, Nojima M, Iwaki H, Nobuoka T, Nishida T, Miyazaki Y, Takamaru H, et al. 2010. A novel correlation between LINE-1 hypomethylation and the malignancy of gastrointestinal stromal tumors. *Clin Cancer Res* **16:** 5114–5123.

Jiang Z, Jhunjhunwala S, Liu J, Haverty PM, Kennemer MI, Guan Y, Lee W, Carnevali P, Stinson J, Johnson S, et al. 2012. The effects of hepatitis B virus integration into the genomes of hepatocellular carcinoma patients. *Genome Res* **22:** 593–601.

Kan Z, Zheng H, Liu X, Li S, Barber TD, Gong Z, Gao H, Hao K, Willard MD, Xu J, et al. 2013. Whole-genome sequencing identifies recurrent mutations in hepatocellular carcinoma. *Genome Res* **23:** 1422–1433.

Kearse M, Moir R, Wilson A, Stones-Havas S, Cheung M, Sturrock S, Buxton S, Cooper A, Markowitz S, Duran C, et al. 2012. Geneious Basic: an integrated and extendable desktop software platform for the organization and analysis of sequence data. *Bioinformatics* **28:** 1647–1649.

Kim CM, Koike K, Saito I, Miyamura T, Jay DG. 1991. HBx gene of hepatitis B virus induces liver cancer in transgenic mice. *Nature* **351:** 317–320.

Koike K, Moriya K, Iino S, Yotsuyanagi H, Endo Y, Miyamura T, Kurokawa K. 1994. High-level expression of hepatitis B virus HBx gene and hepatocarcinogenesis in transgenic mice. *Hepatology* **19:** 810–819.

Lau C-C, Sun T, Ching AK, He M, Li JW, Wong AM, Co NN, Chan AW, Li PS, Lung RW, et al. 2014. Viral-human chimeric transcript predisposes risk to liver cancer development and progression. *Cancer Cell* **25:** 335–349.

Li S, Mao M. 2013. Next generation sequencing reveals genetic landscape of hepatocellular carcinomas. *Cancer Lett* **340:** 247–253.

Lupberger J, Hildt E. 2007. Hepatitis B virus–induced oncogenesis. *World J Gastroenterol* **13:** 74–81.

Minami M, Poussin K, Brechot C, Paterlini P. 1995. A novel PCR technique using *Alu*-specific primers to identify unknown flanking sequences from the human genome. *Genomics* **29:** 403–408.

Mirabello L, Sun C, Ghosh A, Rodriguez AC, Schiffman M, Wentzensen N, Hildesheim A, Herrero R, Wacholder S, Lorincz A, et al. 2012. Methylation of human papillomavirus type 16 genome and risk of cervical precancer in a Costa Rican population. *J Natl Cancer Inst* **104:** 556–565.

Murakami Y, Minami M, Daimon Y, Okanoue T. 2004. Hepatitis B virus DNA in liver, serum, and peripheral blood mononuclear cells after the clearance of serum hepatitis B virus surface antigen. *J Med Virol* **72:** 203–214.

Nakagawa H, Shibata T. 2013. Comprehensive genome sequencing of the liver cancer genome. *Cancer Lett* **340:** 234–240.

Oishi Y, Watanabe Y, Yoshida Y, Sato Y, Hiraishi T, Oikawa R, Maehata T, Suzuki H, Toyota M, Niwa H, et al. 2012. Hypermethylation of Sox17 gene is useful as a molecular diagnostic application in early gastric cancer. *Tumour Biol* **33:** 383–393.

Orend G, Kuhlmann I, Doerfler W. 1991. Spreading of DNA methylation across integrated foreign (adenovirus type 12) genomes in mammalian cells. *J Virol* **65:** 4301–4308.

Schriml LM, Padilla-Nash HM, Coleman A, Moen P, Nash WG, Menninger J, Jones G, Ried T, Dean M. 1999. Tyramide signal amplification (TSA)-FISH applied to mapping PCR-labeled probes less than 1 kb in size. *Biotechniques* **27:** 608–613.

Sells MA, Chen ML, Acs G. 1987. Production of hepatitis B virus particles in Hep G2 cells transfected with cloned hepatitis B virus DNA. *Proc Natl Acad Sci* **84:** 1005–1009.

Speel EJ, Ramaekers FC, Hopman AH. 1997. Sensitive multicolor fluorescence in situ hybridization using catalyzed reporter deposition (CARD) amplification. *J Histochem Cytochem* **45:** 1439–1446.

Sung WK, Zheng H, Li S, Chen R, Liu X, Li Y, Lee NP, Lee WH, Ariyaratne PN, Tennakoon C, et al. 2012. Genome-wide survey of recurrent HBV integration in hepatocellular carcinoma. *Nat Genet* **44:** 765–769.

Taniguchi Y, Nosaka K, Yasunaga J, Maeda M, Mueller N, Okayama A, Matsuoka M. 2005. Silencing of human T-cell leukemia virus type I gene transcription by epigenetic mechanisms. *Retrovirology* **2:** 64.

Tao Q, Robertson KD. 2003. Stealth technology: how Epstein-Barr virus utilizes DNA methylation to cloak itself from immune detection. *Clin Immunol* **109:** 53–63.

Toh ST, Jin Y, Liu L, Wang J, Babrzadeh F, Gharizadeh B, Ronaghi M, Toh HC, Chow PK, Chung AY, et al. 2013. Deep sequencing of the hepatitis B virus in hepatocellular carcinoma patients reveals enriched integration events, structural alterations and sequence variations. *Carcinogenesis* **34:** 787–798.

Toyota M, Ho C, Ahuja N, Jair KW, Li Q, Ohe-Toyota M, Baylin SB, Issa JP. 1999. Identification of differentially methylated sequences in colorectal cancer by methylated CpG island amplification. *Cancer Res* **59:** 2307–2312.

Uozaki H, Fukayama M. 2008. Epstein-Barr virus and gastric carcinoma-viral carcinogenesis through epigenetic mechanisms. *Int J Clin Exp Pathol* **1:** 198–216.

Watanabe Y, Castoro RJ, Kim HS, North B, Oikawa R, Hiraishi T, Ahmed SS, Chung W, Cho MY, Toyota M, et al. 2011. Frequent alteration of MLL3 frameshift mutations in microsatellite deficient colorectal cancer. *PLoS ONE* **6:** e23320.

Yamada Y, Ito T. 2011. Highly efficient PCR assay to discriminate allelic DNA methylation status using whole genome amplification. *BMC Res Notes* **4:** 179.

Received March 8, 2014; accepted in revised form December 29, 2014.

Toxicology and Applied Pharmacology 282 (2015) 237–243

Contents lists available at ScienceDirect

Toxicology and Applied Pharmacology

journal homepage: www.elsevier.com/locate/ytaap

Mitochondrial iron accumulation exacerbates hepatic toxicity caused by hepatitis C virus core protein

Shuichi Sekine [a], Konomi Ito [a], Haruna Watanabe [a], Takafumi Nakano [a], Kyoji Moriya [b], Yoshizumi Shintani [b], Hajime Fujie [b], Takeya Tsutsumi [b], Hideyuki Miyoshi [b], Hidetake Fujinaga [b], Seiko Shinzawa [b], Kazuhiko Koike [b], Toshiharu Horie [a,*]

[a] Laboratory of Biopharmaceutics, Graduate School of Pharmaceutical Sciences, Chiba University, 1-8-1 Inohana, Chuo-ku, Chiba 260-8675, Japan
[b] Department of Internal Medicine, Graduate School of Medicine, The University of Tokyo, 7-3-1 Hongo, Bunkyo-ku, Tokyo 113-8655, Japan

ARTICLE INFO

Article history:
Received 8 September 2014
Revised 9 December 2014
Accepted 16 December 2014
Available online 27 December 2014

Keywords:
Ca^{2+} uniporter
Fenton reaction
Reactive oxygen species
Ru360
Hepatitis C virus

ABSTRACT

Patients with long-lasting hepatitis C virus (HCV) infection are at major risk of hepatocellular carcinoma (HCC). Iron accumulation in the livers of these patients is thought to exacerbate conditions of oxidative stress. Transgenic mice that express the HCV core protein develop HCC after the steatosis stage and produce an excess of hepatic reactive oxygen species (ROS). The overproduction of ROS in the liver is the net result of HCV core protein-induced dysfunction of the mitochondrial respiratory chain. This study examined the impact of ferric nitrilacetic acid (Fe-NTA)-mediated iron overload on mitochondrial damage and ROS production in HCV core protein-expressing HepG2 (human HCC) cells (Hep39b cells). A decrease in mitochondrial membrane potential and ROS production were observed following Fe-NTA treatment. After continuous exposure to Fe-NTA for six days, cell toxicity was observed in Hep39b cells, but not in mock (vector-transfected) HepG2 cells. Moreover, mitochondrial iron (^{59}Fe) uptake was increased in the livers of HCV core protein-expressing transgenic mice. This increase in mitochondrial iron uptake was inhibited by Ru360, a mitochondrial Ca^{2+} uniporter inhibitor. Furthermore, the Fe-NTA-induced augmentation of mitochondrial dysfunction, ROS production, and cell toxicity were also inhibited by Ru360 in Hep39b cells. Taken together, these results indicate that Ca^{2+} uniporter-mediated mitochondrial accumulation of iron exacerbates hepatocyte toxicity caused by the HCV core protein.

Introduction

Hepatitis C virus (HCV) infection is a major cause of chronic liver disease. About 120–200 million people are infected with HCV, increasing their risk of developing chronic hepatitis, cirrhosis, and eventually hepatocellular carcinoma (HCC) (Ikeda et al., 1998; Nishioka et al., 1991). The HCV genome is approximately 9.6 kb in size and encodes a polyprotein of ~3000 amino acids. The large HCV polyprotein is cleaved by host and viral proteases to generate at least ten smaller proteins, including four structural proteins (one core protein, two envelope proteins, and the E1, E2, and p7 ion channels) (Bukh et al., 1995) and six non-structural proteins (NH2-NS2, NS3, NS4A, NS4B, NS5A, and NS5B-COOH) (Bartenschlager and Lohmann, 2000). These proteins participate in viral replication and also influence cellular functions of the host.

Oxidative stress is commonly observed following HCV infection and is caused by increased levels of cellular reactive oxygen species (ROS) or by changes in cellular antioxidant capacities (Choi and Ou, 2006; Oberley, 2002; Otani et al., 2005). In particular, HCV core protein is known to be closely associated with the mitochondria and causes the increase in host ROS production, lipid peroxidation (Lau et al., 1998; Moriya et al., 2001; Okuda et al., 2002) and mitochondrial Ca^{2+} uptake. HCV core protein also reduces GSH and NADPH concentrations and mitochondrial complex I activities. These undertakings ultimately disrupt mitochondrial membrane permeability and trigger mitochondrial dysfunction (Wang et al., 2010; Wang and Weinman, 2006). As mitochondrial function is the master regulator of cellular energy and apoptotic cell death, mitochondrial injury can culminate in metabolic deficits and steatohepatitis, further exacerbating cell injury and dysfunction.

Due to the relationship between chronic HCV infection and the development of HCC, numerous studies have attempted to identify the HCV proteins that are responsible for hepatocarcinogenesis. These studies indicate that the HCV core protein can promote the immortalization of primary human hepatocytes (Ray et al., 2000), whereas the non-

Abbreviations: HCV, hepatitis C virus; HCC, hepatocellular carcinoma; ROS, reactive oxygen species; Fe-NTA, ferric nitrilacetic acid; JC-1, 5,5′,6,6′-tetrachrolo-1,1′,3,3′-tetraethylbenzimidazoly-carbocyanine iodide; CCCP, carbonyl cyanide-m-chlorophenyl hydrazine; MTT, 3-(4,5-dimethylthiazol-2-yl)-2,5-diphenyltetrazolium bromide; HPF, hydroxyphenyl fluorescein; ANT, adenine nucleotide translocator; HRP, horseradish peroxidase; DMEM, Dulbecco's Modified Eagle's Medium; CL, chemiluminescence; TTBS, Tris-buffered saline/0.05% Tween 20; BSA, bovine serum albumin; Hep39b, HCV core protein-expressing HepG2; Hepswx, vector-transfected HepG2.

* Corresponding author at: Faculty of Pharmaceutical Sciences, Teikyo Heisei University, 4-21-2 Nakano, Nakano-ku, Tokyo 164-8530, Japan. Fax: +81 3 5860 4237.
E-mail address: t.horie@thu.ac.jp (T. Horie).

http://dx.doi.org/10.1016/j.taap.2014.12.004
0041-008X/

structural proteins NS3 and NS4B can transform NIH 3T3 cells, either individually or in combination with Ha-ras (Park et al., 2000). Iron overload in the liver, which is associated with the genetic disorder hereditary hemochromatosis, has been thought to increase the risk of HCC by about 200-fold (Bonkovsky et al., 1997; Kowdley, 2004). For example, the livers of patients afflicted with HCV are characterized by the elevated expression of transferrin receptor 1 and hepcidin, both of which stimulate iron uptake into hepatocytes (Bonkovsky et al., 1997; Hayashi et al., 1994). In contrast, iron depletion (in the form of dietary iron restriction and/or phlebotomy) can improve hepatic inflammation and lower serum aminotransferase activity in HCV patients (Hayashi et al., 1994). Thus, a major precipitating factor for the pathogenesis of HCV-related liver disease has been attributed to the augmentation of oxidative stress following iron accumulation. However, no underlying cellular mechanism has yet been elucidated.

This study investigated the effect of iron exposure on mitochondrial dysfunction, ROS production and cell toxicity in human hepatoma cells stably expressing the HCV core protein (Hep39b cells). The underlying mechanism responsible for mitochondrial iron accumulation in Hep39b cells and in the livers of HCV core protein-expressing transgenic mice was also examined.

Materials and methods

Chemicals and reagents. Ferric nitrate nonahydrate, nitrilotriacetic acid (NTA), 5,5′,6,6′-tetrachrolo-1,1′,3,3′-tetraethylbenzimidazolylcarbocyanine iodide (JC-1), carbonyl cyanide-m-chlorophenyl hydrazine (CCCP) and G418 disulfate were from Sigma Aldrich (St. Louis, MO). MitoTracker® Red was from Invitrogen (Carlsbad, CA). $^{59}FeSO_4$ was from Perkin-Elmer (Waltham, MA). Ru360 was from Merck Millipore Japan (Tokyo, Japan). MTT [3-(4,5-dimethylthiazol-2-yl)-2,5-diphenyltetrazolium bromide] was from Wako Pure Chemical Industries, Ltd. (Osaka, Japan). Hydroxyphenyl fluorescein (HPF) was from Sekisui Medical Co., Ltd. (Tokyo, Japan). Adenine nucleotide translocator (ANT) goat polyclonal IgG, CCDC109A goat polyclonal IgG and horseradish peroxidase (HRP)-conjugated anti-goat IgG were from Santa Cruz Biotechnology, Inc. (Santa Cruz, CA). All chemicals and solvents were of analytical grade.

Preparation of Fe-NTA. The Fe-NTA complex was prepared as described by Awai et al. (1979). Briefly, ferric nitrate was dissolved in 1 N HCl to form a 50 mM solution, and NTA was dissolved in 1 N NaOH to form a 150 mM solution. Equal volumes of the two solutions were mixed just before the experiment, and the pH was adjusted to 7.4 with $NaHCO_3$.

Assessment of cytotoxicity. Cytotoxicity was assessed by the MTT assay. Briefly, Hep39b and Hepswx cells were seeded into 96 well culture plates at a density of 8.4×10^3 cells/well and were exposed to various concentrations of Fe-NTA the following day, the medium was replaced with fresh medium containing the same component every 24 h. In some conditions, cells were treated with 20 μM Ru360, a mitochondrial Ca^{2+} uniporter inhibitor, for 1 h prior to Fe-NTA exposure. After six days, the cell culture medium was replaced by 50 μl MTT solution (5 mg/ml MTT in phenol red-free Dulbecco's Modified Eagle's Medium (DMEM)), and the cells were incubated for 2 h at 37 °C. To dissolve the reduced MTT crystals, 200 μl isopropanol was added. The absorbance of the dye was measured at a wavelength of 570 nm, and the turbidity of the cells (background absorbance) was measured at a reference wavelength of 630 nm. The absorbance of the controls (Hepswx and Hep39b) was set at 100%, and cytotoxicity was calculated as the absorbance of the experimental sample relative to that of the control.

Assessment of ROS production. ROS production was first assessed by chemiluminescence (CL) analysis. Briefly, cells were seeded into 35 mm glass-bottomed dishes at a density of 2.5×10^5 cells/dish and exposed to 300 μM Fe-NTA the following day, the medium was replaced with fresh medium containing the same component every 24 h. In some cases, cells were treated with Ru360 for 1 h prior to Fe-NTA treatment. After five days, the cell culture medium was replaced with phenol red-free DMEM containing Fe-NTA and Ru360, and the dish was protected from light. The following day, spontaneous CL was measured using a single photoelectron counting system (CLD-10; Tohoku Electronic Industrial Co., Ltd., Sendai, Japan), as described previously (Maeda et al., 2010). Emission was expressed in counts/10 min/mg protein.

ROS production was also assessed using HPF as a fluorescent probe for the selective detection of hydroxyl radicals. Briefly, cells were seeded into 35 mm glass-bottomed dishes, as described for CL analysis. After 7 days, the cell culture medium was replaced with modified Hanks' balanced salt solution (HBSS) containing 10 mM HEPES, 1 mM $MgCl_2$, 2 mM $CaCl_2$ and 2.7 mM glucose (pH 7.4). Next, 10 μM HPF and 20 nM MitoTracker® Red (a fluorescent probe for the mitochondria) were added, and cells were incubated for 15 min at 37 °C. Images of HPF and MitoTracker® Red staining were obtained using a laser scanning confocal microscope (FV300; Olympus Optical Co., Ltd., Tokyo, Japan). The wavelengths (excitation/emission) for the detection of HPF (green) and MitoTracker® Red (red) were 488 nm/515 nm and 579 nm/599 nm, respectively.

Assessment of mitochondrial membrane potential. Measurement of mitochondrial membrane potential was performed using the JC-1 stain, a lipophilic cation fluorescent dye that accumulates in the mitochondria. At a low mitochondrial membrane potential, the JC-1 dye exists as a monomeric molecule and fluoresces green, whereas at a higher membrane potential the JC-1 dye forms polymeric aggregates and fluoresces red. A fall in the mitochondrial membrane potential is therefore indicated by a decrease in the ratio of red signal to green signal.

Cells were cultured in 96 well black culture plates at a density of 8.4×10^3 cells/well and exposed to various concentrations of Fe-NTA the following day, the medium was replaced with fresh medium containing the same component every 24 h. After six days, the culture medium was replaced with 200 μl JC-1 solution (10 μg/ml JC-1 in HBSS), and cells were incubated in the dark for 30 min at 37 °C. After washing twice with HBSS, the absorbance of the cells in each well was immediately measured using a fluorescence plate reader with the excitation and emission wavelengths set at 490 nm and 530 nm (green)/590 nm (red), respectively.

Animals. The production of transgenic mice expressing the HCV core protein has been described previously (Moriya et al., 2001). Briefly, the HCV core protein gene was placed downstream of a transcriptional regulatory region from the hepatitis B virus and introduced into C57BL/6 mouse embryos (Clea Japan, Tokyo, Japan). All of the animals were treated humanely in accordance with the guidelines issued by the National Institute of Health and all procedures described below were approved by the animal care committee of Chiba University.

Isolation of mouse liver mitochondria. The mouse liver mitochondrial fraction was prepared according to a previously described method (Masubuchi et al., 2002). Livers were isolated from two mice and placed in ice-cold buffer containing 250 mM sucrose, 10 mM HEPES–KOH, and 0.5 mM EGTA (pH 7.4). Livers were cut into small cubes with scissors in the same buffer and homogenized five times with a Potter homogenizer. The homogenates were diluted to 0.25 g liver/ml and were centrifuged at 770 ×*g* for 5 min at 4 °C. The resulting supernatant was decanted and further centrifuged at 9800 ×*g* for 10 min. The pellet was resuspended to yield a concentration of 0.5 g liver/ml in buffer containing 250 mM sucrose, 10 mM HEPES–KOH and 0.3 mM EGTA (pH 7.4), and centrifuged at 4500 ×*g* for 10 min. The pellet was resuspended to yield a concentration of 1 g liver/ml in the same buffer and centrifuged at 2000 ×*g* for 2 min, followed by further centrifugation at 4500 ×*g* for 8 min. The

final pellet was then resuspended in buffer containing 250 mM sucrose and 10 mM HEPES–KOH (pH 7.4) and used for further experiments.

Mitochondrial iron uptake. All experiments were conducted in a 30 °C water bath. After pre-incubation of the mitochondria in buffer containing 225 mM sucrose, 10 mM KCl, 5 mM $MgCl_2$, 5 mM KH_2PO_4, and 20 mM Tris–HCl (pH 7.4) for 1 min, Ru360 was added at a final concentration of 10 μM, $^{59}FeSO_4$ was added after 1 min, and the ^{59}Fe remaining in the mitochondria after 10 min was measured using a gamma counter.

Western blotting analysis. The mouse liver mitochondrial fraction (10 μg protein) was subjected to electrophoresis on a 12.5% polyacrylamide slab gel containing 0.1% sodium dodecyl sulfate and transferred onto an Immobilon-P Transfer Membrane filter (Millipore Corporation, Billerica, MA). The membrane was blocked for 1 h at room temperature with Tris-buffered saline/0.05% Tween 20 (TTBS) containing 3% bovine serum albumin (BSA) and probed overnight at 4 °C with the CCDC109A goat polyclonal IgG (1:200) against the Ca^{2+} uniporter and the ANT goat polyclonal IgG (1:1000). The membrane was then incubated for 1 h at room temperature with donkey anti-goat IgG-HRP (1:3333). All antibodies were diluted in TTBS containing 0.1% BSA. Immunoreactive bands were detected using a LAS-1000 imaging system (Fuji Film, Tokyo, Japan) and an enhanced CL system (GE Healthcare, Little Chalfont, Buckinghamshire, UK).

Statistical analysis. All data are represented as the mean ± the standard error (S.E.). Data were statistically analyzed by using one-way ANOVA followed by the Bonferroni test for multiple comparison. For comparison among two groups, two-tailed Student's t-test was adopted. Differences between means at the level of $P < 0.05$ were considered significant.

Results

Iron-induced cytotoxicity in HCV core protein-expressing HepG2 cells

The iron uptake system is perturbed in HCV-infected hepatocytes due to elevated expression of transferrin receptor 1. However, because of its hydrophobicity, Fe-NTA is taken up into the cell in a transferrin receptor 1-independent manner by passive diffusion. Fe-NTA is then converted into free Fe^{2+} by several types of esterases. Therefore, Fe-NTA was used in the current study to control for intrinsic differences in active iron uptake between HCV core protein-expressing HepG2 cells (Hep39b cells) and vector-transfected HepG2 cells (Hepswx cells). After treatment with Fe-NTA for six days, cytotoxicity was assessed using the MTT assay. Concentration-dependent cytotoxicity of Fe-NTA against Hep39b cells was observed. By contrast, no cytotoxicity was observed against control Hepswx cells at Fe-NTA concentrations of less than 1000 μM (Fig. 1). These data indicate that HCV core protein expression affects the susceptibility of hepatocytes to Fe-NTA-induced iron cytotoxicity.

Effect of iron accumulation on ROS production in HCV core protein-expressing versus control hepatocytes

To directly measure free radical formation, we took advantage of methodology for measuring spontaneous CL and compared the levels of CL in HCV core protein-expressing Hep39b and control Hepswx cells (Fig. 2a). As shown in Fig. 2a, spontaneous CL was significantly higher in Hep39b cells by approximately 156% compared with that in Hepswx cells (6015 versus 3856 arbitrary units; $P < 0.01$). In the presence of 300 μM Fe-NTA, iron-induced CL was also significantly higher in Hep39b cells relative to Hepswx cells (2.61-fold versus 1.54-fold increase; $P < 0.01$ and $P < 0.001$, respectively) (Fig. 2a).

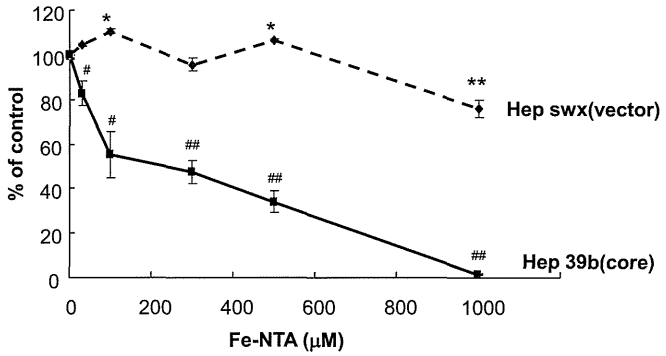

Fig. 1. Iron-induced cytotoxicity in control versus HCV core protein-expressing hepatocytes. Hepswx (dashed line) and Hep39b (solid line) cells were exposed with Fe-NTA (30, 100, 300, 500 and 1000 μM) for six days. Hepatotoxicity was determined using the MTT assay. Viability was calculated as the absorbance of the experimental sample relative to that of the controls (without Fe-NTA treatments). Values are the mean ± the S.E. $^{*}P < 0.05$ and $^{**}P < 0.01$, significantly different from the control (without Fe-NTA). $^{\#}P < 0.05$ and $^{\#\#}P < 0.01$, significantly different from respective control cells (Hepswx) ($n = 6$).

Effect of iron accumulation on mitochondrial ROS production

Mitochondria are a major source of ROS production. Therefore, we next examined the production of mitochondrial hydroxyl radicals by free iron catalyzation (i.e., the Fenton reaction). Since increased production of ROS was observed in Hep39b cells in the presence of Fe-NTA, we next examined mitochondrial ROS production by double staining with MitoTracker® Red (red), a fluorescent probe for the mitochondria, and HPF (green), a fluorescent probe for the selective detection of hydroxyl radicals. As shown in Fig. 2b, a strong fluorescent signal derived from HPF was observed in Hep39b cells in the presence of Fe-NTA. This fluorescence overlapped with that generated by MitoTracker® Red (Fig. 2b). The fluorescent signal derived from HPF in overlapped area was significantly higher in Hep39b cells by approximately 200% compared with that in Hepswx cells (Fig. 2c). These data indicate that mitochondrial hydroxyl radical production was increased in the presence of the HCV core protein and Fe-NTA.

Effect of HCV core protein on mitochondrial membrane potential

The HCV core protein is known to inhibit mitochondrial respiratory complex I activity (Korenaga et al., 2005). Inhibition of complex I leads to ROS formation due to premature electron leakage from the complex. Therefore, we next examined the effect of Fe-NTA on mitochondrial membrane potential in Hep39b cells by using JC-1, a lipophilic cationic dye that selectively enters the mitochondria and reversibly changes color from green to red as the membrane potential increases. Fig. 3 demonstrates that the mitochondrial membrane potential was decreased in HCV core protein-expressing Hep39b cells compared with control Hepswx cells. The decrease in membrane potential was significantly increased following exposure to Fe-NTA (300 and 1000 μM) for six days (Fig. 3).

Mitochondrial free iron uptake in HCV core protein-expressing versus control hepatocytes

Because mitochondrial hydroxyl radical production was increased in the presence of Fe-NTA (Fig. 2), the uptake of free iron into isolated mitochondria was next examined. To ensure a sufficient quantity and quality of the mitochondria for this experiment, mitochondria were isolated from the liver of HCV core protein-expressing transgenic and wild-type (control) mice. Fig. 4 shows that the concentration of mitochondrial free

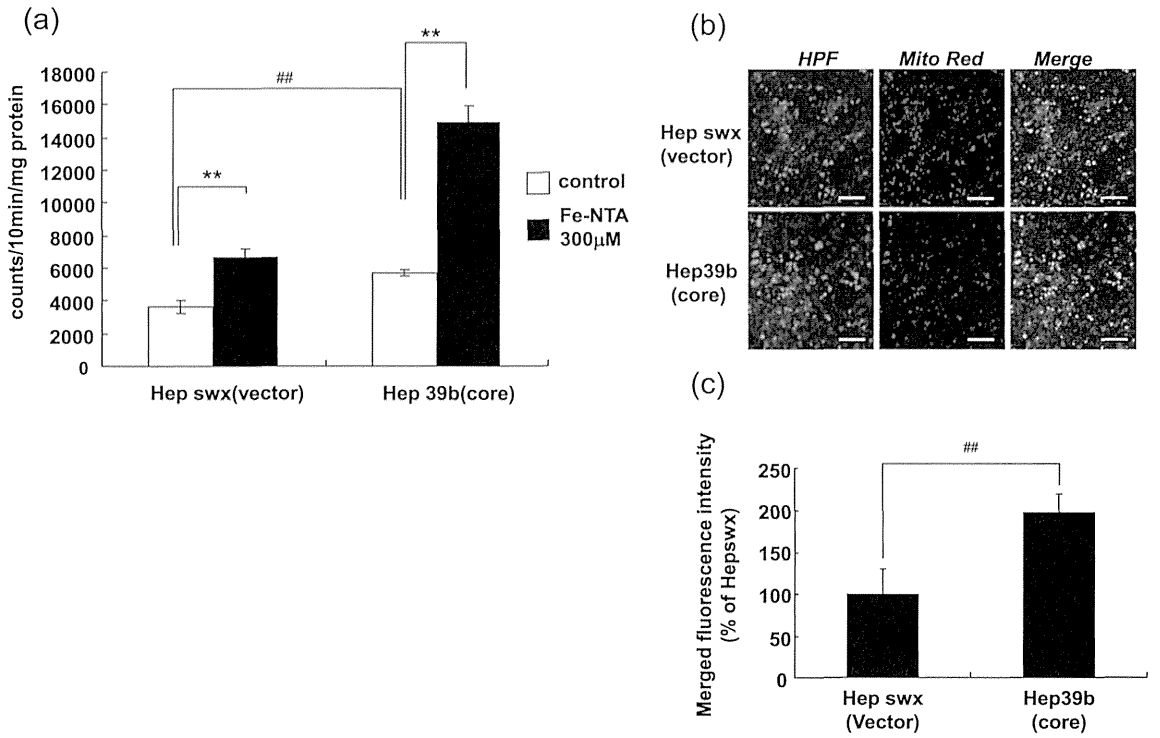

Fig. 2. Iron-induced mitochondrial ROS production is enhanced in HCV core protein-expressing hepatocytes. (a) Hepswx and Hep39b cells were exposed to Fe-NTA (300 μM) for six days. ROS production was determined using a CL analyzer. Detected counts were normalized by protein content of cell lysate. Values are given as the mean ± the S.E. $^{**}P < 0.01$ and $^{\#\#}P < 0.01$, significantly different from respective control (n = 3–4). (b) Hepswx and Hep39b cells were pretreated with HPF (green) and MitoTracker® Red (red). Mitochondrial ROS production was determined by the strength of yellow fluorescence in the merged pictures. The scale bar represents 100 μm. (c) Analysis of merged fluorescence microscopy images was done by ImageJ. Integrated density of merged area was automatically selected and fluorescence intensity of HPF was calculated within the merged area of 200–300 cells.

iron ($^{59}Fe^{2+}$) was significantly increased in the mitochondria derived from the transgenic versus the control mouse liver (62.2 ± 4.2 versus 79.5 ± 2.1 pmol/mg protein, respectively; $P < 0.05$), whereas the passive diffusion of $^{59}Fe^{2+}$ into the mitochondria (estimated by $^{59}Fe^{2+}$ uptake at 4 °C) was 31.1 ± 3.2 pmol/10 min/mg protein in Hepswx cells, and 29.2 ± 1.8 pmol/10 min/mg protein in Hep39b cells (not significantly different). Moreover, $^{59}Fe^{2+}$ uptake into the transgenic and control mitochondria was attenuated to the same level by Ru360 (48.2 ± 4.1 versus 47.5 ± 1.2 pmol/mg protein, respectively) (Fig. 4). These data indicate that calcium uniporter plays a role in free iron uptake into the mitochondria and that the activity of the Ca^{2+} uniporter is increased by the HCV core protein.

Effect of Ru360 on Fe-NTA-induced ROS production and cytotoxicity

We next examined the effect of Ru360 on Fe-NTA-induced ROS production and cytotoxicity in Hep39b versus Hepswx cells. As shown in Fig. 5a, in the absence of Fe-NTA, Ru360 had no effect on ROS production

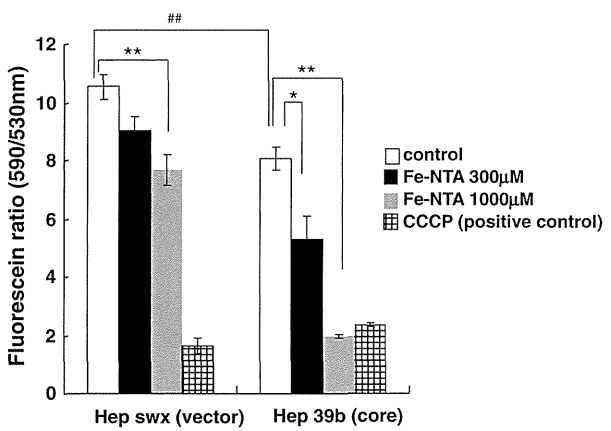

Fig. 3. The iron-induced reduction in mitochondrial membrane potential is increased by the expression of HCV core protein. Hepswx and Hep39b cells were exposed to Fe-NTA for six days. Mitochondrial membrane potential was estimated fluorometrically. Values are given as the mean ± the S.E. $^{*}P < 0.05$, $^{**}P < 0.01$ and $^{\#\#}P < 0.01$, significantly different from respective control (n = 6).

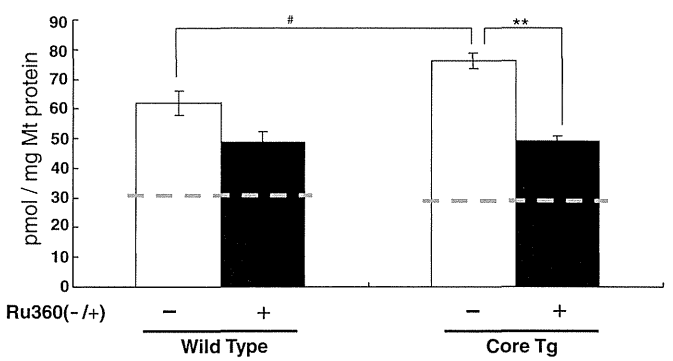

Fig. 4. Mitochondrial iron uptake is augmented by the expression of HCV core protein and inhibited by Ru360. Mitochondria were isolated from wild-type and HCV core protein transgenic (Tg) mice and exposed to $^{59}FeSO_4$ with/without Ru360. Free iron uptake was measured in the isolated mitochondria and the free iron uptake amount was normalized by mitochondrial protein content. The dashed line represents the passive diffusion into the mitochondria. Values are given as the mean ± the S.E. $^{**}P < 0.01$ and $^{\#}P < 0.05$, significantly different from respective control (n = 3–8).

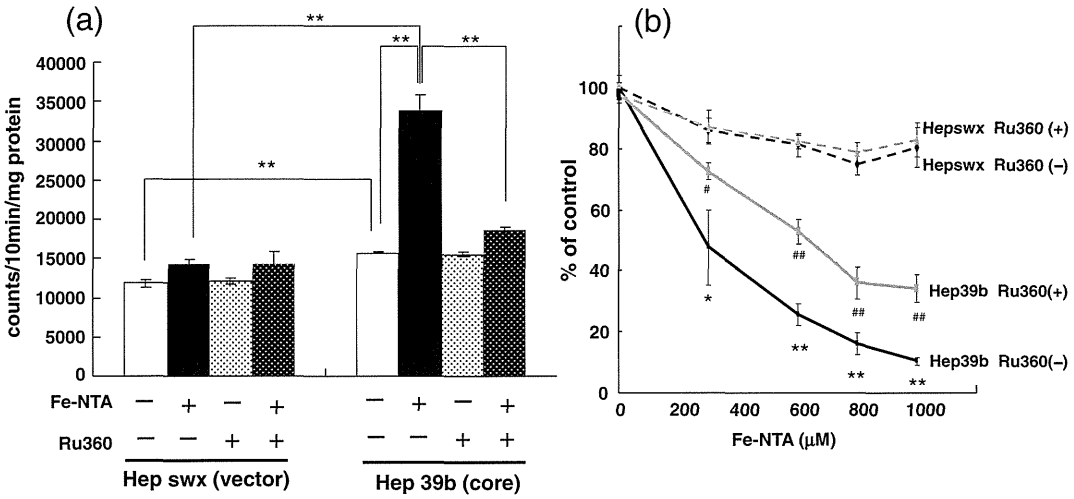

Fig. 5. Iron-induced ROS production and cytotoxicity are inhibited by Ru360 in HCV core protein-expressing hepatocytes. (a) Hepswx and Hep39b cells were exposed to Fe-NTA (300 μM) and Ru360 (20 μM) for six days. ROS production was determined using a CL analyzer. Values are given as the mean ± the S.E. $^{**}P < 0.01$, significantly different from respective control (n = 8). (b) Hepswx and Hep39b cells were exposed to Fe-NTA (300, 600, 800, and 1000 μM) and Ru360 (20 μM) for six days. Cytotoxicity was determined using the MTT assay. Values are given as the mean ± the S.E. $^{*}P < 0.05$ and $^{**}P < 0.01$, significantly different from Hepswx Ru360(−). $^{\#}P < 0.05$ and $^{\#\#}P < 0.01$, significantly different from Hep39b Ru360(−) (n = 6).

in Hepswx cells and Hep39b cells. On the other hand, Ru360 significantly suppressed Fe-NTA (300 μM)-induced ROS production in Hep39b but not Hepswx cells (Fig. 5a). Moreover, cytotoxicity following exposure to (300, 600, 800 and 1000 μM) Fe-NTA for six days was also specifically inhibited by Ru360 treatment in Hep39b cells (Fig. 5b).

Expression of the Ca^{2+} uniporter in isolated mitochondria

Given that mitochondrial free iron uptake is enhanced in HCV core protein-expressing Hep39b cells (Fig. 4), we next examined the expression of the Ca^{2+} uniporter in the mitochondria isolated from the liver of HCV core protein-expressing transgenic mice relative to control mice. As shown in Fig. 6, mitochondrial expression of the uniporter was similar in transgenic versus control mice, as assessed by Western blot analysis.

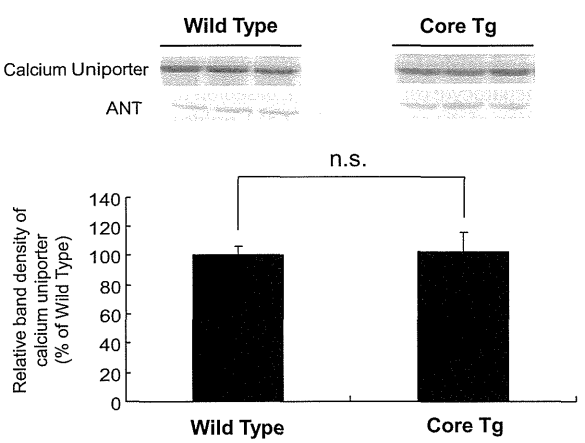

Fig. 6. Expression of mitochondrial Ca^{2+} uniporter in the livers of HCV core protein-expressing transgenic versus wild-type mice. Mitochondria were isolated from the livers of wild-type (control) and HCV core protein-expressing transgenic (Tg) mice. The expression levels of the Ca^{2+} uniporter and ANT (loading control) were determined by Western blot analysis. Mitochondrial proteins (10 μg) were loaded into each lane of the gel. The band density of the uniporter was normalized to the band density of ANT. Values are given as the mean ± the S.E. n.s.: not significantly different (n = 3).

Discussion

The accumulation of iron into the liver of HCV core protein-expressing transgenic mice fed a normal diet is similar to that observed in chronic HCV patients (Farinati et al., 1995; Kato et al., 2001). On the other hand, the expression level of hepcidin, which regulates iron metabolism by inhibiting iron absorption from the intestine and the hepatic portal system, is reportedly decreased in the liver of HCV patients and full-length HCV genome-expressing transgenic mice, but not in the liver of HCV core protein-expressing transgenic mice (Moriya et al., 2010; Muckenthaler, 2008). Therefore, although the precise regulation of iron transport into the mitochondria is essential for heme biosynthesis, hemoglobin production, and Fe–S clustering, the mechanism(s) behind mitochondrial iron homeostasis is not yet fully understood.

Previous work from our group revealed elevated ROS generation in HCV core protein-expressing transgenic mice (Moriya et al., 2001). Moreover, our previous work, along with that of others (Korenaga et al., 2005), showed that the core protein interacts with the outer mitochondrial membrane and impairs the mitochondrial respiratory chain in the normal mouse liver via inhibition of complex I activity (unpublished data). Inhibition of respiratory chain complexes ultimately leads to the overproduction of ROS via electron leakage from the mitochondria. Therefore, we hypothesized that the inducible mitochondrial iron transport system exacerbates hepatic toxicity caused by the HCV core protein.

This study employed Fe-NTA to exclude intrinsic differences in iron uptake into HCV core protein-expressing Hep39b cells and vector-transfected Hepswx cells. In addition, we demonstrated that HCV core protein-induced alterations in mitochondrial ROS production and membrane potential were augmented in the presence of iron (Figs. 2 and 3). These data may indicate that iron-dependent mitochondrial dysfunction was amplified via the Fenton reaction, which produces potent reactive free radicals (i.e., hydroxyl radicals) (Fig. 7).

Iron is absolutely essential for the sustenance of all forms of life due to its unusual ability to serve as both an electron donor and acceptor. On the other hand, free iron is also potentially toxic, which is related to its ability to donate and accept electrons within the cell. Free iron catalyzes the conversion of hydrogen peroxide into free radicals, which can cause damage to the mitochondria and cellular structures. For this reason, the iron homeostasis is strictly regulated, and the impairment of iron homeostasis is related to several diseases. In patients with HCV, hepatic

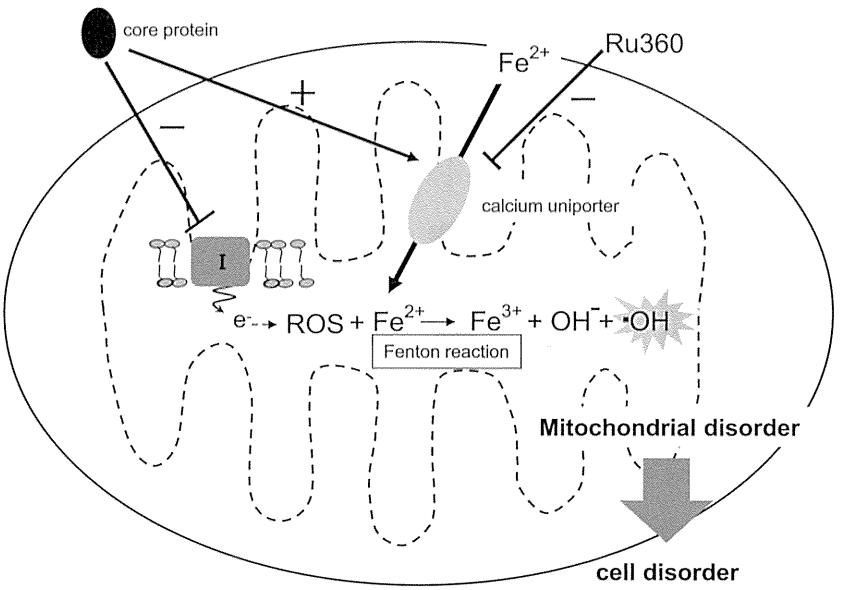

Fig. 7. Proposed mechanism of mitochondrial iron accumulation and hepatic cytotoxicity caused by the HCV core protein. The HCV core protein induces mitochondrial ROS production by inhibiting mitochondrial complex I. In addition, it is suggested that the HCV core protein stimulates mitochondrial iron uptake through the mitochondrial Ca^{2+} uniporter. The excess iron then leads to mitochondrial ROS production and mitochondrial/cellular malfunction/disorder when the HCV core protein is expressed.

and serum free iron concentrations are ~7-fold higher (12.5 mmol/g liver and 134 mg/dl, respectively) than those of a normal individual (Farinati et al., 1995; Kageyama et al., 1998; Olynyk et al., 1995; Silva et al., 2005). In this study, significant hepatotoxicity was observed at 30 μM Fe-NTA in HCV core protein-expressing Hep39b cells (Fig. 1). Therefore, a physiologically relevant concentration of iron (30 μM), which is not sufficient to induce cell toxicity by itself, was synergistic with the toxic actions of the core protein (Fig. 1). This interplay was similarly revealed by the synergy between iron and the core protein in inducing mitochondrial dysfunction and ROS production (Figs. 2 and 3).

This study further demonstrated that mitochondrial free iron uptake was partially mediated by the Ca^{2+} uniporter. The Ca^{2+} uniporter was selectively inhibited by Ru360 and exhibited an increased capacity to uptake iron into HCV core protein-expressing liver mitochondria versus normal liver mitochondria (Fig. 4). However, the expression of the uniporter was unaltered in core protein-expressing transgenic mice relative to normal mice (Fig. 6). Li et al. (2007) reported that the activity of the Ca^{2+} uniporter was up-regulated in the presence of the core protein: The in vitro incubation of mouse liver mitochondria with HCV core protein (100 ng/mg) increased the Ca^{2+} entry rate by ~2-fold. The Ca^{2+} uniporter is located in the inner mitochondrial membrane and transports not only Ca^{2+} but also other metal cationic ions (e.g., Fe^{2+}) into the mitochondrial matrix space in a mitochondrial membrane potential-dependent fashion (Bernardi, 1999).

Iron uptake was significantly suppressed to the same level by Ru360 in the mitochondria isolated from both core protein-expressing transgenic and normal mice (Fig. 4). Moreover, as free iron uptake into the mitochondria was still observed at 4 °C for both types of the mitochondria, about half of the iron (Hepswx; 31.1 ± 3.2 pmol/10 min/mg protein, Hep39b; 29.2 ± 1.8 pmol/10 min/mg protein) was estimated to enter into the mitochondria by passive diffusion (Fig. 4, dashed line). These data indicate that the up-regulation of iron uptake in the mitochondria isolated from transgenic mice was mediated by the HCV core protein-induced stimulation of Ru360-sensitive Ca^{2+} uniporter transport activity. However, the mechanism by which the core protein alters the function of the mitochondrial uniporter is still unclear, especially given that the core protein binds to the outer mitochondrial membrane, and the uniporter is located in the inner mitochondrial membrane. It is known that mitochondrial calcium uniporter possibly forms multi-molecular complex (Raffaello et al., 2012). Mitochondrial calcium uniporter function could be altered by the effect on essential regulator and/or protein involved in the assembly of the channel. In this regard, though our current study demonstrated that HCV core protein had no effect on Ca^{2+} uniporter expression (Fig. 6), it is possible that other mechanisms are involved in the HCV core protein-induced stimulation of Ca^{2+} uniporter transport activity. Further study should be addressed in the future.

Interferon-α has been used as monotherapy for chronic hepatitis C, yet only about 40–50% of hepatitis C patients experience an initial biochemical response to the cytokine. Interestingly, high iron accumulation in chronic HCV carriers is related to a poor response to interferon therapy (Walters et al., 1973). In addition, some investigators have suggested that iron removal therapy (via phlebotomy or food therapy (i.e., restriction of an iron rich-diet)) can attenuate liver damage in hepatitis C patients by still unknown mechanisms (Hayashi et al., 1994; Kato et al., 2007). The current study showed that the HCV core protein-induced mitochondrial iron uptake is responsible for exacerbating mitochondrial dysfunction and ROS production, which finally seems to lead to hepatocyte toxicity (Fig. 7). Based on these results, we suggest that inhibition of the mitochondrial Ca^{2+} uniporter may provide a new therapeutic approach to treat liver disease in HCV patients.

Conflict of interest statement

The authors declare no conflict of interest.

Acknowledgments

This work was supported by a grant-in-aid for scientific research (A) 548 (21249003) and a grant-in-aid for young scientists (B) (21790141) from the Ministry of Education, Culture, Sports, Science and Technology of Japan.

References

Awai, M., Narasaki, M., Yamanoi, Y., Seno, S., 1979. Induction of diabetes in animals by parenteral administration of ferric nitrilotriacetate. A model of experimental hemochromatosis. Am. J. Pathol. 95, 663–673.

Bartenschlager, R., Lohmann, V., 2000. Replication of hepatitis C virus. J. Gen. Virol. 81, 1631–1648.
Bernardi, P., 1999. Mitochondrial transport of cations: channels, exchangers, and permeability transition. Physiol. Rev. 79, 1127–1155.
Bonkovsky, H.L., Banner, B.F., Rothman, A.L., 1997. Iron and chronic viral hepatitis. Hepatology 25, 759–768.
Bukh, J., Miller, R.H., Purcell, R.H., 1995. Genetic heterogeneity of hepatitis C virus: quasispecies and genotypes. Semin. Liver Dis. 15, 41–63.
Choi, J., Ou, J.H., 2006. Mechanisms of liver injury. III. Oxidative stress in the pathogenesis of hepatitis C virus. Am. J. Physiol. Gastrointest. Liver Physiol. 290, G847–G851.
Farinati, F., Cardin, R., De Maria, N., Della Libera, G., Marafin, C., Lecis, E., et al., 1995. Iron storage, lipid peroxidation and glutathione turnover in chronic anti-HCV positive hepatitis. J. Hepatol. 22, 449–456.
Hayashi, H., Takikawa, T., Nishimura, N., Yano, M., Isomura, T., Sakamoto, N., 1994. Improvement of serum aminotransferase levels after phlebotomy in patients with chronic active hepatitis C and excess hepatic iron. Am. J. Gastroenterol. 89, 986–988.
Ikeda, K., Saitoh, S., Suzuki, Y., Kobayashi, M., Tsubota, A., Koida, I., et al., 1998. Disease progression and hepatocellular carcinogenesis in patients with chronic viral hepatitis: a prospective observation of 2215 patients. J. Hepatol. 28, 930–938.
Kageyama, F., Kobayashi, Y., Murohisa, G., Shimizu, E., Suzuki, F., Kikuyama, M., et al., 1998. Failure to respond to interferon-alpha 2a therapy is associated with increased hepatic iron levels in patients with chronic hepatitis C. Biol. Trace Elem. Res. 64, 185–196.
Kato, J., Kobune, M., Nakamura, T., Kuroiwa, G., Takada, K., Takimoto, R., et al., 2001. Normalization of elevated hepatic 8-hydroxy-2′-deoxyguanosine levels in chronic hepatitis C patients by phlebotomy and low iron diet. Cancer Res. 61, 8697–8702.
Kato, J., Miyanishi, K., Kobune, M., Nakamura, T., Takada, K., Takimoto, R., et al., 2007. Long-term phlebotomy with low-iron diet therapy lowers risk of development of hepatocellular carcinoma from chronic hepatitis C. J. Gastroenterol. 42, 830–836.
Korenaga, M., Wang, T., Li, Y., Showalter, L.A., Chan, T., Sun, J., et al., 2005. Hepatitis C virus core protein inhibits mitochondrial electron transport and increases reactive oxygen species (ROS) production. J. Biol. Chem. 280, 37481–37488.
Kowdley, K.V., 2004. Iron, hemochromatosis, and hepatocellular carcinoma. Gastroenterology 127, S79–S86.
Lau, J.Y., Xie, X., Lai, M.M., Wu, P.C., 1998. Apoptosis and viral hepatitis. Semin. Liver Dis. 18, 169–176.
Li, Y., Boehning, D.F., Qian, T., Popov, V.L., Weinman, S.A., 2007. Hepatitis C virus core protein increases mitochondrial ROS production by stimulation of Ca^{2+} uniporter activity. FASEB J. 21, 2474–2485.
Maeda, T., Miyazono, Y., Ito, K., Hamada, K., Sekine, S., Horie, T., 2010. Oxidative stress and enhanced paracellular permeability in the small intestine of methotrexate-treated rats. Cancer Chemother. Pharmacol. 65, 1117–1123.
Masubuchi, Y., Nakayama, S., Horie, T., 2002. Role of mitochondrial permeability transition in diclofenac-induced hepatocyte injury in rats. Hepatology 35, 544–551.
Moriya, K., Nakagawa, K., Santa, T., Shintani, Y., Fujie, H., Miyoshi, H., et al., 2001. Oxidative stress in the absence of inflammation in a mouse model for hepatitis C virus-associated hepatocarcinogenesis. Cancer Res. 61, 4365–4370.
Moriya, K., Miyoshi, H., Shinzawa, S., Tsutsumi, T., Fujie, H., Goto, K., et al., 2010. Hepatitis C virus core protein compromises iron-induced activation of antioxidants in mice and HepG2 cells. J. Med. Virol. 82, 776–792.
Muckenthaler, M.U., 2008. Fine tuning of hepcidin expression by positive and negative regulators. Cell Metab. 8, 1–3.
Nishioka, K., Watanabe, J., Furuta, S., Tanaka, E., Iino, S., Suzuki, H., et al., 1991. A high prevalence of antibody to the hepatitis C virus in patients with hepatocellular carcinoma in Japan. Cancer 67, 429–433.
Oberley, T.D., 2002. Oxidative damage and cancer. Am. J. Pathol. 160, 403–408.
Okuda, M., Li, K., Beard, M.R., Showalter, L.A., Scholle, F., Lemon, S.M., et al., 2002. Mitochondrial injury, oxidative stress, and antioxidant gene expression are induced by hepatitis C virus core protein. Gastroenterology 122, 366–375.
Olynyk, J.K., Reddy, K.R., Di Bisceglie, A.M., Jeffers, L.J., Parker, T.I., Radick, J.L., et al., 1995. Hepatic iron concentration as a predictor of response to interferon alfa therapy in chronic hepatitis C. Gastroenterology 108, 1104–1109.
Otani, K., Korenaga, M., Beard, M.R., Li, K., Qian, T., Showalter, L.A., et al., 2005. Hepatitis C virus core protein, cytochrome P450 2E1, and alcohol produce combined mitochondrial injury and cytotoxicity in hepatoma cells. Gastroenterology 128, 96–107.
Park, J.S., Yang, J.M., Min, M.K., 2000. Hepatitis C virus nonstructural protein NS4B transforms NIH3T3 cells in cooperation with the Ha-ras oncogene. Biochem. Biophys. Res. Commun. 267, 581–587.
Raffaello, A., De Stefani, D., Rizzuto, R., 2012. The mitochondrial Ca^{2+} uniporter. Cell Calcium 52, 16–21.
Ray, R.B., Meyer, K., Ray, R., 2000. Hepatitis C virus core protein promotes immortalization of primary human hepatocytes. Virology 271, 197–204.
Silva, I.S., Perez, R.M., Oliveira, P.V., Cantagalo, M.I., Dantas, E., Sisti, C., et al., 2005. Iron overload in patients with chronic hepatitis C virus infection: clinical and histological study. J. Gastroenterol. Hepatol. 20, 243–248.
Walters, G.O., Miller, F.M., Worwood, M., 1973. Serum ferritin concentration and iron stores in normal subjects. J. Clin. Pathol. 26, 770–772.
Wang, T., Weinman, S.A., 2006. Causes and consequences of mitochondrial reactive oxygen species generation in hepatitis C. J. Gastroenterol. Hepatol. 21 (Suppl. 3), S34–S37.
Wang, T., Campbell, R.V., Yi, M.K., Lemon, S.M., Weinman, S.A., 2010. Role of hepatitis C virus core protein in viral-induced mitochondrial dysfunction. J. Viral Hepat. 17, 784–793.

Cancer Cell
Article

ER Stress Cooperates with Hypernutrition to Trigger TNF-Dependent Spontaneous HCC Development

Hayato Nakagawa,[1,5,8] Atsushi Umemura,[1,8] Koji Taniguchi,[1] Joan Font-Burgada,[1] Debanjan Dhar,[1] Hisanobu Ogata,[1,6] Zhenyu Zhong,[1] Mark A. Valasek,[2] Ekihiro Seki,[3] Juan Hidalgo,[4] Kazuhiko Koike,[5] Randal J. Kaufman,[7] and Michael Karin[1,2,*]

[1]Laboratory of Gene Regulation and Signal Transduction, Department of Pharmacology
[2]Department of Pathology
[3]Department of Medicine
School of Medicine, University of California, San Diego, 9500 Gilman Drive, San Diego, CA 92093, USA
[4]Department of Cell Biology, Physiology and Immunology, Institute of Neurosciences, Universitat Autonoma de Barcelona, Bellaterra, 08193 Barcelona, Spain
[5]Department of Gastroenterology, University of Tokyo, 7-3-1 Hongo, Bunkyo-ku, Tokyo 113-8655, Japan
[6]Department of Medicine and Clinical Science, Graduate School of Medical Sciences, Kyushu University, Fukuoka 812-8582, Japan
[7]Program in Degenerative Diseases, Sanford-Burnham Medical Research Institute, 10901 North Torrey Pines Road, La Jolla, CA 92037, USA
[8]Co-first author
*Correspondence: karinoffice@ucsd.edu
http://dx.doi.org/10.1016/j.ccr.2014.07.001

SUMMARY

Endoplasmic reticulum (ER) stress has been implicated in the pathogenesis of viral hepatitis, insulin resistance, hepatosteatosis, and nonalcoholic steatohepatitis (NASH), disorders that increase risk of hepatocellular carcinoma (HCC). To determine whether and how ER stress contributes to obesity-driven hepatic tumorigenesis we fed wild-type (*WT*) and *MUP-uPA* mice, in which hepatocyte ER stress is induced by plasminogen activator expression, with high-fat diet. Although both strains were equally insulin resistant, the *MUP-uPA* mice exhibited more liver damage, more immune infiltration, and increased lipogenesis and, as a result, displayed classical NASH signs and developed typical steatohepatitic HCC. Both NASH and HCC development were dependent on TNF produced by inflammatory macrophages that accumulate in the *MUP-uPA* liver in response to hepatocyte ER stress.

INTRODUCTION

Hepatocellular carcinoma (HCC) is the fifth most common cancer worldwide and a leading cause of cancer deaths. More than 90% of HCC develops in the context of chronic liver disease, with hepatitis B virus (HBV) or hepatitis C virus (HCV) infections being the main causes. However, 30%–40% of Western HCC patients do not exhibit viral infections (El-Serag, 2011). Most of these patients are obese with manifestations of the metabolic syndrome and suffer from nonalcoholic steatohepatitis (NASH), a severe form of nonalcoholic fatty-liver disease (NAFLD) (Cohen et al., 2011). Indeed, obesity increases male HCC risk by up to 4.5-fold (Calle et al., 2005) and also increases HCC risk in viral hepatitis (Chen et al., 2008). Because the prevalence of obesity has been increasing worldwide, its association with hepatocarcinogenesis has attracted much attention. In previous studies, we have shown that feeding mice exposed to the hepatic carcinogen diethylnitrosamine (DEN) with high-fat diet (HFD) strongly enhanced HCC development (Park et al., 2010). Although low-grade liver inflammation associated with tumor necrosis factor (TNF) and interleukin-6 (IL-6) expression contributes to obesity-promoted HCC development in this model, it should be noted that wild-type (*WT*) mice do not develop NASH, even after DEN administration and prolonged HFD feeding. It is therefore not clear whether the mechanism identified in DEN-treated mice has much bearing on NASH-driven human HCC (Toffanin et al., 2010).

Significance

ER stress is often observed in cancer, but its role in tumorigenesis has not been explored. ER stress also occurs in premalignant liver diseases, including NASH, which progress to HCC, a highly aggressive and common cancer. Our work demonstrates that, when combined with hypernutrition, ER stress of liver parenchymal cells results in NASH-like disease that spontaneously progresses to HCC through an inflammatory mechanism dependent on TNF and IκB kinase signaling.

In considering possible mechanisms through which obesity may promote HCC development, we decided to study the potential contribution of ER stress because obesity (Hotamisligil, 2010; Ozcan et al., 2006) and HBV/HCV infections (Malhi and Kaufman, 2011) result in liver ER stress, which promotes hepatosteatosis (Rutkowski et al., 2008). Furthermore, several ER stress markers are elevated in NASH-affected livers (Puri et al., 2008), and it was suggested that ER stress causes ballooning degeneration of the hepatocytes, a classical sign of NASH (Caldwell et al., 2010). To this end, we placed *MUP-uPA* mice, which express high amounts of urokinase plasminogen activator (uPA) specifically in the hepatocytes and therefore undergo transient ER stress (Sandgren et al., 1991; Weglarz et al., 2000), and *WT* mice on a HFD. Whereas the *WT* mice developed simple steatosis and no HCC, the *MUP-uPA* mice developed NASH-like disease that spontaneously progressed to HCC, whose development was dependent on TNF production by inflammatory liver macrophages and TNF receptor 1 (TNFR1)-IκB kinase β (IKKβ) signaling in hepatocytes. Our results suggest that NASH and progression to steatohepatitic HCC may be prevented or ameliorated by anti-TNF drugs.

RESULTS

HFD Induces NASH Signs and Spontaneous HCC in *MUP-uPA* Mice

WT and *MUP-uPA* mice were placed on a HFD (60% of calories were fat derived), starting at 6 weeks of age. Body weight and glucose intolerance did not differ between the two strains (Figures S1A and S1B available online). As reported (Weglarz et al., 2000), the serum alanine aminotransferase (ALT) level in *MUP-uPA* mice on a normal-chow diet (low-fat diet [LFD]) was markedly elevated at 5 weeks of age but rapidly declined, probably due to the replacement of dying hepatocytes with new cells in which uPA expression was extinguished (Sandgren et al., 1991; Weglarz et al., 2000) (Figure S1C). However, HFD feeding maintained high serum ALT throughout the observation period (Figure 1A), even though it did not restore uPA expression (Figure S1C). By contrast, in *WT* mice the HFD substantially elevated the ALT after only 32 weeks, and it reached a level similar to *MUP-uPA* mice at 40 weeks. Examination of the liver histology revealed hepatocyte damage, evidenced by tissue clearing, in 5-week-old *MUP-uPA* mice, but this had almost disappeared at 24 weeks on the LFD, except for mild inflammation and spotty necrosis (Figure 1B). As reported (Park et al., 2010), HFD-fed *WT* mice showed pronounced steatosis but little inflammation by 24 weeks (Figure 1B). At that time, HFD-fed *MUP-uPA* mice exhibited extensive immune infiltration into the liver and numerous ballooning hepatocytes, both of which are important diagnostic features of human NASH (Brunt, 2001). Furthermore, HFD-fed *MUP-uPA* mice showed pericellular and bridging fibrosis, resembling the pattern in human NASH (Figure 1C; Figure S1D). This was accompanied by the increased expression of type 1 collagen α1 mRNA (Figure S1E).

Terminal deoxynucleotidyl transferase-mediated deoxyuridine triphosphate nick-end labeling (TUNEL) staining showed that both apoptotic (nuclear fragmentation) and necrotic (diffuse cytoplasmic staining) cell death were significantly increased in HFD-fed *MUP-uPA* livers and that, as a result, the numbers of Ki67-positive proliferating hepatocytes and K19-positive cells were also elevated (Figure 1D). The expression of cyclin D1 was also increased (Figure S1F). Thus, HFD-fed *MUP-uPA* mice exhibit continuous hepatocyte death and compensatory proliferation, a critical process in hepatocarcinogenesis (Maeda et al., 2005).

HFD-fed *MUP-uPA* mice developed small tumors on the liver surface by 32 weeks of age and large tumors at 40 weeks (Figure 2A; Figures S2A and S2B), when 78.6% (11/14 mice) of HFD-fed *MUP-uPA* mice had tumors larger than 2 mm and 35.7% (5/14 mice) had tumors larger than 10 mm. Histologically, 30% of tumors larger than 2 mm were HCCs, similar to human steatohepatitic HCC, a histotype describing NASH-related HCC with ballooning cancer cells and inflammatory cell infiltration (Salomao et al., 2012), although some displayed a classical thick trabecular pattern, whereas the remaining 70% were either typical or steatohepatic adenomas (Figure 2B; Figures S2C and S2D). Cancer cells were highly proliferative and frequently positive for α fetoprotein (AFP) with marked p62 aggregation (Figure S2E), a sign of impaired autophagy frequently observed in human HCC (Inami et al., 2011). Several oncogenic mediators, such as extracellular signal regulated-kinase (ERK), signal transducer and activator of transcription 3 (STAT3), and c-Jun N-terminal kinase (JNK), as well as cyclin D1, the liver oncogenes Yes-associated protein 1 (YAP) and Myc, and the cancer stem cell markers epithelial cellular adhesion molecule (EpCAM) and CD44, were activated or upregulated (Figures S2F–S2H). By contrast, 30% of LFD-fed *MUP-uPA* mice displayed a few tiny nodules in the liver even at 40 weeks of age, corresponding to simple hyperplasia (Figure S2C). Although 1 of 11 LFD-fed *MUP-uPA* mice developed a small 3 mm tumor, the tumor was also classified as hyperplasia, which is not proliferative and is AFP negative (Figures S2C and S2I). In *WT* mice, neither the LFD nor HFD induced any liver tumors by 40 weeks. Of note, HFD-fed *MUP-uPA* mice showed microscopically visible foci of p62- and YAP-positive cells already at 24 weeks (Figure S2J). These foci may contain progenitors to the tumors detected at 32–40 weeks. Thus, HFD feeding of *MUP-uPA* mice induced complete NASH-like pathological features with continuous hepatocyte death and compensatory proliferation, and eventually led to spontaneous HCC and adenoma development, which were not seen in the LFD-maintained mice.

ER Stress Enhances Lipogenesis and Aggravates Steatohepatitis

Although the mechanism responsible for hepatocyte death in young *MUP-uPA* mice is not entirely clear, their hepatocytes are ER stressed (Sandgren et al., 1991). Indeed, several ER stress markers, including C/EBP homologous protein (CHOP), glucose-regulated protein 78 (GRP78), spliced X-box binding protein 1 (sXBP1), phosphorylated eIF2α (p-eIF2α), phosphorylated inositol-requiring enzyme 1α (p-IRE1α), and phosphorylated JNK (p-JNK), were elevated in 5-week-old *MUP-uPA* mice compared to *WT* (Figure 3A; Figure S3A). Whereas in 16-week-old *MUP-uPA* mice most markers declined, paralleling the decline in uPA expression, HFD-fed *MUP-uPA* mice maintained strong eIF2α and JNK phosphorylation and CHOP expression (Figure 3B; Figure S3A). In *WT* mice, HFD feeding induced only a slight elevation in p-eIF2α and CHOP mRNA, with no effect on CHOP protein (Figure 3B). Using

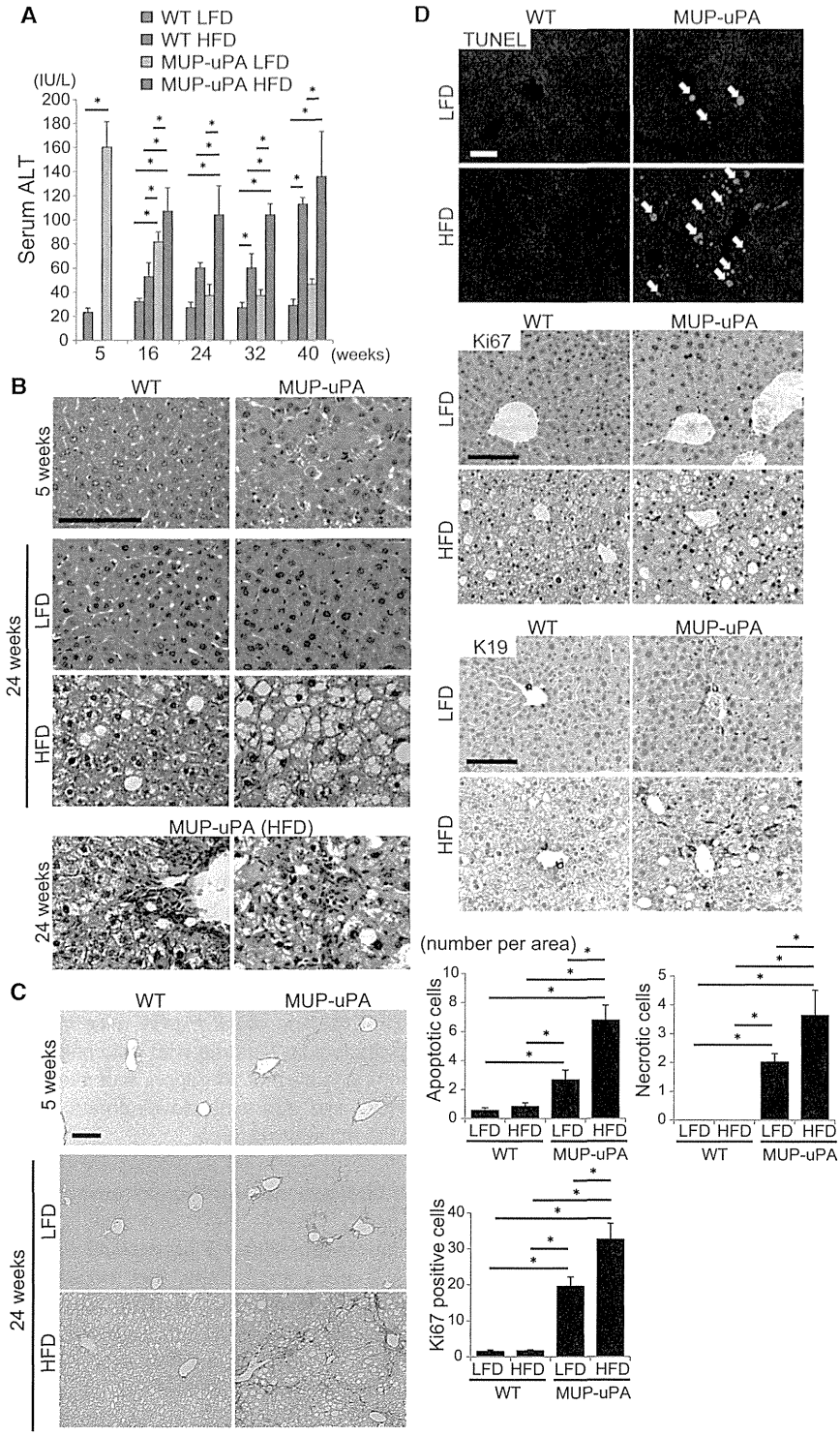

Figure 1. HFD-Fed *MUP-uPA* Mice Display Classical NASH Signs

(A) Serum ALT in LFD- or HFD-fed *WT* and *MUP-uPA* mice was measured at indicated ages. HFD feeding was initiated at 6 weeks. Data are means ± SD (n = 3–5 per group). *p < 0.05.

(B) H&E staining of liver sections from 5-week-old mice on the LFD and 24-week-old mice kept on the LFD or HFD (scale bar, 100 μm). The bottom two panels show the infiltration of immune cells in HFD-fed *MUP-uPA* mouse livers (left, portal area; right, liver parenchyma).

(C) Sirius Red staining of liver sections described in (B) (scale bar, 100 μm).

(D) TUNEL and IHC analyses of Ki67 and K19 in 24-week-old mice that were kept on the LFD or HFD (scale bar, 100 μm). Yellow and white arrows indicate apoptotic and necrotic cells, respectively. Bar graphs show the numbers of apoptotic and necrotic cells and Ki67-positive cells per 200X field. Data are means ± SD (n = 5 per group). *p < 0.05.

See also Figure S1.

immunohistochemistry (IHC), we confirmed the level of nuclear CHOP in the hepatocytes of 5-week-old *MUP-uPA* mice, which was sustained at 16 weeks of age only in the HFD-fed *MUP-uPA* mice (Figure 3C). Tribble3 (TRB3) and death receptor 5 (DR5), two molecules capable of inducing cell death, were highly upregulated in *MUP-uPA* mice, especially after HFD feeding (Figure S3B). After 24 weeks of the HFD, expression of the DR5 ligand TNF-related apoptosis-inducing ligand (TRAIL) was also elevated in the *MUP-uPA* liver. Electron microscopy (EM) revealed distended and dilated ERs in HFD-fed *MUP-uPA* mice (Figure S3C). Thus, whereas ER stress appears to be induced by uPA expression in 5-week-old *MUP-uPA* mice, it declines due to transgene extinction. However, feeding these mice with HFD rekindles the stress response and induces several cell-death mediators that are not expressed in HFD-fed *WT* mice. To determine whether ER stress can cause ballooning degeneration and hepatocyte death, we injected HFD-fed *WT* mice with the protein-glycosylation inhibitor and ER-stress elicitor tunicamycin. This treatment led to rapid (36 hr) induction of ballooning degeneration, hepatocyte apoptosis, and ALT release only in the HFD-fed mice (Figures S3D–S3F). The white appearance of the liver from HFD-fed mice treated with tunicamycin suggested that the liver had become more steatotic.

These results are consistent with the ability of ER stress to cause liver steatosis (Rutkowski et al., 2008). Indeed, Oil Red O (ORO) staining showed mild spontaneous lipid accumulation in 5-week-old *MUP-uPA* mice, which diminished by 16 weeks of age under the LFD (Figure 3D). However, HFD feeding induced more extensive lipid accumulation in the *MUP-uPA* than in the *WT* mice. Liver triglycerides (TGs) and cholesterol were also elevated (Figure 3E). Decreased liver lipid export due to the suppression of apolipoprotein B (apoB) expression/secretion and increased lipogenesis were suggested

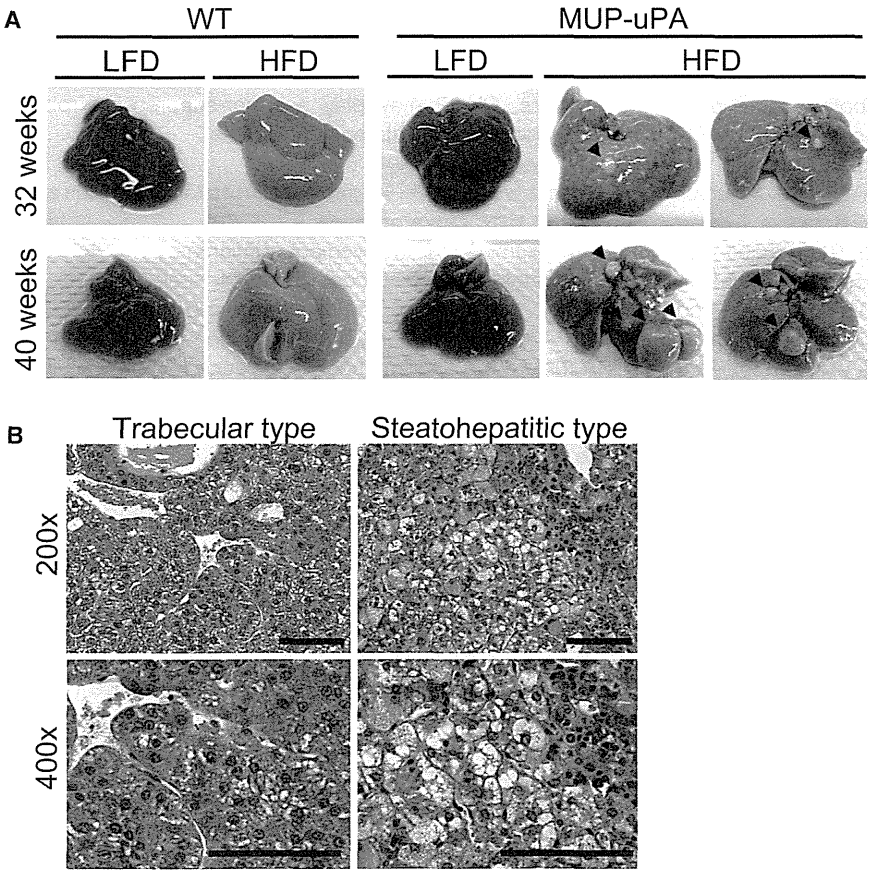

Figure 2. NASH to HCC Progression in *MUP-uPA* Mice

(A) Representative images of livers from 32- and 40-week-old mice that were kept on the LFD or HFD.

(B) Representative H&E staining of tumor sections from 40-week-old HFD-fed *MUP-uPA* mice. The left two panels show trabecular HCC, and the right two panels show steatohepatitic HCC (scale bar, 100 μm).

See also Figure S2.

to be involved in ER stress-induced steatosis (Ota et al., 2008; Qiu et al., 2011; Rutkowski et al., 2008). Because apoB carries TGs and cholesterol from the liver elsewhere, we examined serum TGs and cholesterol and liver apoB mRNA. There were no differences in apoB mRNA among the four groups (Figure S3G), and the serum TGs and total cholesterol were similarly elevated in HFD-fed *WT* and *MUP-uPA* mice (Figure S3H), suggesting that liver lipid export was not fully impaired in *MUP-uPA* mice. Next, we examined the mRNAs of lipogenic regulators. Although sterol regulatory element-binding protein 2 (SREBP2) mRNA was slightly increased and peroxisome proliferator-activated receptor α (PPARα) and CCAAT/enhancer-binding protein α (c/EBPα) mRNAs were slightly decreased in the 5-week-old *MUP-uPA* mice compared to the *WT* mice, these trends were not seen in the 16-week-old mice (Figure S3I). Expression of PPARγ was decreased in the 16-week-old *MUP-uPA* mice but not in the 5-week-old mice. Therefore, the enhanced lipogenesis in *MUP-uPA* mice could not be explained by the differential expression of these molecules. However, among lipogenic regulators, SREBP1 is controlled not only by synthesis but also by cleavage and subsequent nuclear translocation (Goldstein et al., 2006), which are stimulated by ER stress (Kammoun et al., 2009). Indeed, the SREBP1 precursor abundance was decreased in the 5-week-old *MUP-uPA* livers, and mature nuclear SREBP1 was elevated (Figure 3F). HFD feeding further accelerated SREBP1 processing in the *MUP-uPA* mice but also induced some SREBP1 processing in the *WT* mice. The mRNA expression of the SREBP1 target fatty-acid synthase (FAS), was increased in the 5-week-old and HFD-fed *MUP-uPA* mice (Figure 3G). Consistent with elevated lipogenesis, gas chromatography determination of the hepatic fatty-acid (FA) composition revealed a significant increase in C16:0 palmitic acid (PA) and longer-chain FA in *MUP-uPA* mice compared to *WT* mice, which was further enhanced by HFD feeding (Figure 3H). Excess lipid accumulation leads to oxidative stress due to mitochondrial H_2O_2 production, which can induce cell death (Anderson et al., 2009). Accordingly, the HFD-fed *MUP-uPA* mice displayed strong dihydroethidium (DHE) staining of hepatocytes and a decrease in liver reduced glutathione (GSH): oxidized glutathione (GSSG) ratio (Figures 3I and 3J). Oxidative stress in HFD-fed *MUP-uPA* mice may contribute to CHOP expression, JNK activation, lipotoxic hepatocyte death, and oncogenic mutations.

The IRE1α-XBP1 pathway has been reported to regulate the hepatic lipid metabolism via the XBP1-mediated induction of lipogenic enzymes and regulated IRE1-dependent mRNA decay (RIDD) (Lee et al., 2008; So et al., 2012). Although expression of the XBP1 target gene ERdj4 was upregulated in the 5-week-old and HFD-fed *MUP-uPA* mice, there were no differences in expression of diacylglycerol O-acyltransferase 2, a lipogenic enzyme regulated by XBP1 but not by SREBP1 (Figure S3J). RIDD-mediated downregulation of angiopoietein-like protein 3 (Angptl3) and carboxylesterase 1 (Ces1) mRNAs can induce hypolipidemia and hepatosteatosis due to decreased lipid secretion from the liver. Although expression of Angptl3 mRNA was decreased in 5-week-old *MUP-uPA* mice (Figure S3J), there were no differences in serum TGs and total cholesterol levels between the 5-week-old *WT* and *MUP-uPA* mice and in Angptl3 mRNA expression recovered in 16-week-old *MUP-uPA* mice (Figures S3H and S3J). These results suggest that the IRE1-α-XBP1 pathway does not play a major role in NASH development in *MUP-uPA* mice.

Chemical Chaperons and GRP78 Attenuate Lipotoxicity and Lipogenesis in *MUP-uPA* Mice

To examine whether ER stress enhances lipotoxicity in *MUP-uPA* hepatocytes, we incubated *WT* and *MUP-uPA* hepatocytes with PA. After 24 hr, lipotoxic cell death was seen in both *WT* and

MUP-uPA hepatocytes but was more extensive in the latter (Figure 4A). PA increased CHOP expression and SREBP1 maturation in *WT* hepatocytes, but these effects were more pronounced in *MUP-uPA* hepatocytes, which expressed both proteins prior to PA addition (Figure 4B). To examine the contribution of ER stress to these phenomena, we treated hepatocytes with the chemical chaperons 4-phenylbutyrate (4-PBA) and tauro-ursodeoxycholic acid (TUDCA), which reduce ER stress (Ozcan et al., 2006). Both compounds attenuated PA-induced cell death, but their prosurvival effect was more pronounced in *MUP-uPA* hepatocytes (Figure 4A). CHOP induction and SREBP1 maturation upon PA treatment were also reduced by 4-PBA (Figure 4B). Overexpression of the ER protein chaperon GRP78 in *MUP-uPA* hepatocytes also inhibited SREBP1 maturation and PA-induced cell death (Figures 4C and 4D), further supporting the role of ER stress in both phenomena. PA treatment activated JNK, but consistent with previous results that ER stress has only a partial role in JNK activation by PA (Holzer et al., 2011), the effect was restricted to *WT* hepatocytes and 4-PBA treatment only partially reduced JNK phosphorylation (Figure 4B). Nonetheless, the JNK inhibitor D-JNKi protected both cell types from PA-induced death (Figure 4E).

We examined the effect of TUDCA on NASH development. We initiated daily intraperitoneal (i.p.) injections of TUDCA (250 mg/kg) or phosphate-buffered saline (PBS; vehicle control) to the HFD-fed *MUP-uPA* mice at 16 weeks of age. After 4 weeks, hepatosteatosis and hepatocyte ballooning were attenuated (Figure 4F) and serum ALT and hepatic TGs and cholesterol were significantly reduced (Figures 4G–4I). Hepatocyte death and reactive oxygen species (ROS) accumulation were also suppressed (Figures S4A and S4B). TUDCA treatment also inhibited CHOP expression and SREBP1 maturation in livers of the HFD-fed *MUP-uPA* mice (Figure S4C). We also found that in vivo overexpression of GRP78 using an adenovirus vector attenuated hepatic steatosis in the HFD-fed *MUP-uPA* mice (Figures S4D and S4E). However, due to enhanced adenovirus toxicity in *MUP-uPA* mice, we could not assess the effect on NASH and HCC development. Nonetheless, the results suggest that increased lipotoxicity caused by a positively reinforced cycle of ER stress, oxidative stress, and lipogenesis aggravates fatty liver disease in HFD-fed *MUP-uPA* mice.

Given the pronounced expression of CHOP in *MUP-uPA* mice and its postulated role in apoptosis (Malhi and Kaufman, 2011), we crossed *MUP-uPA* mice to $Chop^{\Delta hep}$ mice, in which CHOP was deleted in hepatocytes. Despite efficient CHOP ablation, there was no reduction in liver damage, JNK and eIF2α phosphorylation, or GRP78 expression in young $Chop^{\Delta hep}$/*MUP-uPA* mice (Figures S4F and S4G). Correspondingly, CHOP ablation did not inhibit HCC development (Figure S4H). In fact, CHOP ablation increased tumor multiplicity without affecting tumor size, ER stress markers, or NASH severity (Figures S4I–S4K), results that stand in marked contrast to the protective effect of whole-body *Chop* ablation in DEN-induced hepatocarcinogenesis (DeZwaan-McCabe et al., 2013). CHOP was strongly expressed in some tumors and preneoplastic lesions of HFD-fed *MUP-uPA* mice but not in $Chop^{\Delta hep}$/*MUP-uPA* mice, and the number of TUNEL-positive cells tended to be reduced in the tumor tissues of $Chop^{\Delta hep}$/*MUP-uPA* mice (Figures S4L and S4M), suggesting that hepatocyte CHOP is not positively involved in NASH progression and HCC development, similar to what was observed in whole-body $Chop^{-/-}$ mice on a methionine-choline-deficient (MCD) diet (Soon et al., 2010). Nonetheless, CHOP may play a tumor-suppressive role by inducing apoptosis of initiated hepatocytes.

TNF from Liver Macrophages Promotes Lipogenesis and NASH and HCC Development

Next, we examined the involvement of inflammatory cytokines in hepatosteatosis and steatohepatitis. In 24-week-old mice, TNF and IL-1β, but not IL-6, mRNAs were elevated in HFD-fed *MUP-uPA* livers (Figure 5A). TNF production was confirmed by ELISA (Figure 5B) and immunofluorescence (IF) analysis localized it to F4/80-positive macrophages, whose number was elevated in HFD-fed *MUP-uPA* mouse livers (Figure 5C). The increase in macrophage infiltration and TNF expression was inhibited by TUDCA treatment (Figures S5A and S5B), suggesting that it is stimulated, in part, by hepatocyte ER and oxidative stress.

To investigate the role of TNF in NASH progression and HCC development, we generated TNF receptor 1 (TNFR1)-deficient *MUP-uPA* ($Tnfr1^{-/-}$/*MUP-uPA*) mice. At 5 and 40 weeks of age, there were no differences in liver injury and body weights between the *MUP-uPA* and $Tnfr1^{-/-}$/*MUP-uPA* mice (Figures S5C–S5F). We placed these mice on the HFD from 6 to 40 weeks of age, and assessed the liver histology and tumorigenesis. Body-weight gain at 40 weeks of age was similar between *MUP-uPA* and $Tnfr1^{-/-}$/*MUP-uPA* mice (Figure S5F), but tumor development was substantially reduced upon TNFR1 ablation (Figures 5D and 5E). Importantly, hepatocyte ballooning, ALT release, liver TGs, and cholesterol, as well as SREBP1 and JNK activation, were reduced in the $Tnfr1^{-/-}$/*MUP-uPA* mice (Figures 5F–5I). Therefore, TNFR1 signaling perpetuates NASH pathogenesis and HCC progression.

TNFR1 Signaling Directly Promotes Tumor Growth

To determine whether TNFR1 signaling promotes HCC development by acting in HCC progenitor cells (HcPCs), whose isolation we recently described (He et al., 2013), we transplanted HcPCs from DEN-treated *WT* or $Tnfr1^{-/-}$ mice into *MUP-uPA* mice, which were placed on the LFD or HFD (Figure 6A). The expression of the HcPC marker CD44 was comparable between *WT* and $Tnfr1^{-/-}$ HcPCs (Figure S6A). After 5 months, nontransplanted *MUP-uPA* mice did not have any tumors larger than 2 mm, even after HFD feeding, whereas HcPC-transplanted mice developed multiple HCC nodules (Figure 6B). The HFD feeding did not affect the number of tumors (which was determined by the number of transplanted HcPCs); however, it significantly increased the tumor size in mice transplanted with *WT* HcPCs but not in mice receiving $Tnfr1^{-/-}$ HcPCs (Figures 6B and 6C). Thus, although TNFR1 signaling is dispensable for HcPC induction by DEN, it strongly stimulates tumor growth in a cell-autonomous manner. Control experiments confirmed that TNFR1 was deleted in HCC cells but not in nontumor liver tissues (Figure S6B). In addition, there were no differences in NASH-like pathology and TNF expression in the background liver harboring either *WT* or $Tnfr1^{-/-}$ HcPCs (Figures S6C–S6G). To further investigate the role of TNF signaling in these effects, we treated *WT* HcPC-transplanted *MUP-uPA* mice with the TNF antagonist etanercept

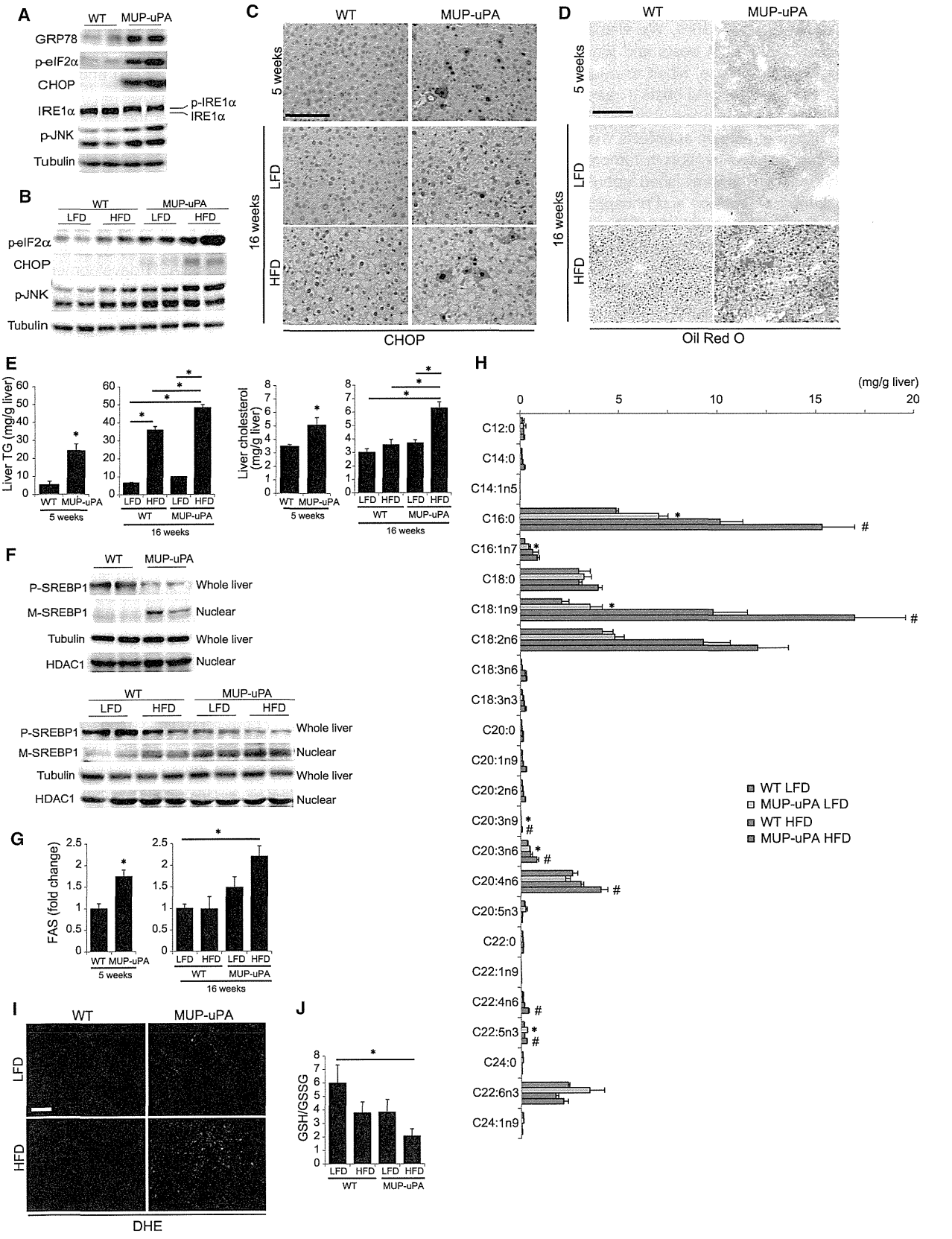

(legend on next page)

under HFD feeding. Etanercept treatment significantly suppressed HCC growth (Figure S6H). We also transplanted *WT* HcPCs into *Tnfr1*$^{-/-}$*/MUP-uPA* hosts and found that the HFD still led to increased tumor size, albeit to a lesser extent than the 2-fold effect seen in *MUP-uPA* hosts (Figure S6I).

We assessed cell proliferation and apoptosis in HcPC-derived tumors. No significant effects on apoptosis were observed, but the HFD enhanced cell proliferation in tumors formed by *WT* HcPCs, and this effect was diminished upon TNFR1 ablation (Figure 6D). Cyclin D1 expression and phosphorylation of ERK, STAT3, JNK, and ribosomal protein S6 (S6) were enhanced by HFD feeding in *WT* HcPC-derived tumors (Figure 6E; Figure S6J). Apart from S6 phosphorylation, these responses were abolished upon TNFR1 ablation. TNFR1 in HcPCs was also required for nuclear factor κ B (NF-κB) activation in tumors that developed in HFD-fed *MUP-uPA* mice (Figure 6F) and IKKβ ablation in HcPC prevented, HFD-enhanced tumor growth (Figure 6G). Thus the TNF-TNFR1-IKKβ-NF-κB pathway is an important mediator of HCC growth in HFD-fed mice.

TNFR1 Signaling Promotes Tumor-Associated Inflammation

Some of the signaling effectors that are activated in HFD-fed mice are not directly regulated by TNFR1. We postulated that autocrine or paracrine signaling may mediate some of the observed responses and analyzed tumors generated by *WT* and *Tnfr1*$^{-/-}$ HcPCs more closely. In HFD-fed mice, both *WT* and *Tnfr1*$^{-/-}$ HCCs were composed of steatotic cells, but immune infiltration was less extensive in *Tnfr1*$^{-/-}$ HCCs (Figure 7A). Real-time PCR and IHC analysis indicated that macrophage and B cell markers were significantly increased by the HFD in *WT* but not in *Tnfr1*$^{-/-}$ HCCs (Figures 7B and 7C). In addition, mRNAs for numerous inflammatory cytokines, chemokines, and growth factors were upregulated by the HFD in *WT* but not in *Tnfr1*$^{-/-}$ HCCs (Figure S7). IF analysis confirmed that expression of chemokine (C-C motif) ligand 7 (CCL7), which attracts macrophages and monocytes, was increased by the HFD in *WT* but not in *Tnfr1*$^{-/-}$ HCCs (Figure 7D). Thus, TNFR1 signaling in HCC cells promotes tumor-associated inflammation, which can account for ERK and STAT3 activation in malignant cells.

DISCUSSION

ER stress and the unfolded protein response (UPR) are upregulated in many cancers and may be associated with drug resistance and adaptation to the transformed state (Wang et al., 2010). Elevated ER stress was also detected in precancerous conditions that precede HCC development, including HBV and HCV infections (Malhi and Kaufman, 2011) and NASH (Farrell et al., 2012; Tilg and Moschen, 2010). However, until recently, researchers have not examined whether the ER stress response, which contributes to insulin resistance and hepatic steatosis (Hotamisligil, 2010), stimulates HCC development. Our results indicate that transient ER stress does not trigger hepatocarcinogenesis in *MUP-uPA* mice that are kept on a LFD but that it elicits a more sustained stress response that also includes extensive oxidative stress when combined with hypernutrition. This response leads to spontaneous NASH development and progression to HCC, whose features closely resemble steatohepatitic HCC in NASH patients. Our studies suggest several potential mechanisms related to ER stress and HFD feeding that cooperate to induce HCC development. First, by stimulating hepatosteatosis (lipid droplet accumulation), HFD sustains a modest degree of ER stress in *MUP-uPA* mice, which otherwise would be switched off upon extinction of uPA expression. Second, ER stress promotes SREBP1 activation, enhancing lipogenesis and increasing the degree of hepatic steatosis beyond what is achieved by HFD alone. Third, ER stress and steatosis increase ROS production in hepatocytes to cause oxidative stress and its sequelae, which include genomic instability, oncogenic mutations, and/or gene-copy-number changes. Fourth, ER and oxidative stress increase the sensitivity of hepatocytes to lipotoxic death, thereby releasing inflammatory mediators that attract and activate monocytes/macrophages. Fifth, TNF and other mediators produced by activated inflammatory macrophages stimulate compensatory hepatocyte proliferation and expand HCC progenitors. TNF further reinforces the inflammatory microenvironment and induces expression of chemokines (CCL2, CCL7, and chemokine [C-X-C motif] ligand 13 [CXCL13]) and growth factors/cytokines (IL-1β, IL-6, TNF itself, lymphotoxin, and hepatocyte growth factor [HGF]) both by HcPCs and surrounding cells. The concerted action of these factors contributes to the development of NASH-like pathology, and NASH contributes to HCC progression. Mutually reinforcing ER stress and hepatosteatosis (Malhi and Kaufman, 2011) are needed to set this pathogenic cascade in motion.

The requirement for two hits (hepatosteatosis and ER stress) for the induction of HCC development in *MUP-uPA* mice resembles that which has been proposed to drive NASH development, a pre-HCC condition, in humans (Day and James, 1998; Tilg and

Figure 3. ER Stress Enhances Lipogenesis and Promotes Steatohepatitis

(A and B) Immunoblot (IB) analysis of ER stress markers in livers of 5-week-old *WT* and *MUP-uPA* mice (A) and 16-week-old *WT* and *MUP-uPA* mice kept on the LFD or HFD (B).

(C) IHC analysis of CHOP in livers of 5-week-old mice on the LFD and 16-week-old mice kept on the LFD or HFD (scale bar, 100 μm).

(D) Oil Red O staining of mouse livers described in (C) (scale bar, 100 μm).

(E) TG and cholesterol content of mouse livers described in (C).

(F) IB analysis of unprocessed precursor SREBP1 (P-SREBP1) in whole liver extract and mature SREBP1 (M-SREBP1) in liver nuclei of mice described in (A) (upper panels) and (B) (lower panels).

(G) Real-time PCR analysis of liver FAS mRNA.

(H) Hepatic FA composition in 16-week-old mice kept on the LFD or HFD, analyzed using gas chromatography. *$p < 0.05$, compared with LFD-fed *WT* mice. #$p < 0.05$, compared with HFD-fed *WT* mice.

(I and J) ROS accumulation in 16-week-old mice that were kept on the LFD or HFD. Images of DHE staining (scale bar, 100 μm) (I) and GSH:GSSG ratio (J) are shown. All bar graphs represent means ± SD ($n = 3$ per group). *$p < 0.05$.

See also Figure S3.

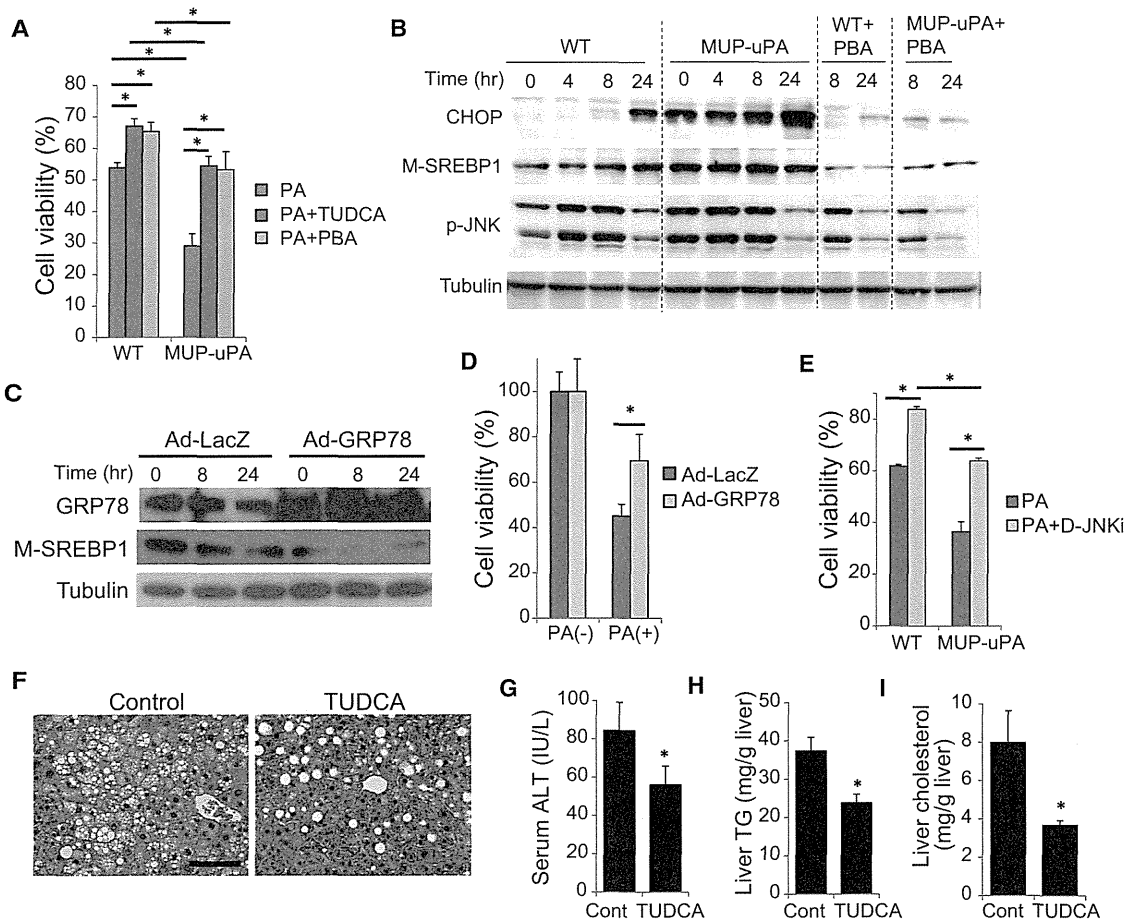

Figure 4. Chemical Chaperons Attenuate Lipotoxicity and Liver Damage in *MUP-uPA* Mice

(A) Primary hepatocytes from *WT* and *MUP-uPA* mice were incubated with 300 μM PA for 24 hr with or without 500 μM TUDCA or 1 mM 4-PBA. Cell viability was assessed using Cell Counting Kit-8 assay. Data are means ± SD of triplicate wells. *$p < 0.05$.

(B) Primary hepatocytes from *WT* and *MUP-uPA* mice were incubated with 200 μM PA with or without 4-PBA as in (A). CHOP expression, SREBP1 maturation, and JNK phosphorylation were assessed using IB.

(C and D) Effect of GRP78 overexpression. *MUP-uPA* hepatocytes were infected with adenoviruses encoding LacZ or GRP78 and then incubated with PA. SREBP1 maturation (C) and cell viability (D) were assessed as in (B).

(E) Hepatocytes from *WT* and *MUP-uPA* mice were incubated with 300 μM PA for 24 hr with or without 10 μM D-JNKi, and cell viability was assessed. Data are means ± SD of triplicate wells. *$p < 0.05$.

(F–I) Effect of TUDCA on NASH in HFD-fed *MUP-uPA* mice. The 16-week-old HFD-fed *MUP-uPA* mice were i.p. injected with TUDCA (250 mg/kg) or the vehicle, and after 4 weeks of daily treatment, liver histology (scale bar, 100 μm) (F), serum ALT (G), liver TGs (H), and liver cholesterol (I) were evaluated. Bar graphs are means ± SD ($n = 5$ per group). *$p < 0.05$.

See also Figure S4.

Moschen, 2010). Although simple steatosis (not NASH) is an extremely common disorder affecting nearly 30% of the US population, only 10%–20% of these patients develop NASH. In the absence of known genetic factors, it was proposed that NASH development depends on multiple secondary hits, which may include microbiota-related factors, food additives, dysbiosis, IL-6 and TNF from adipose tissue, mitochondrial dysfunction, and oxidative or ER stress (Farrell et al., 2012; Tilg and Moschen, 2010). Although these are considered secondary hits, they may act as pre-existing risk factors prior to hepatosteatosis caused by a HFD. Nonetheless, in humans, unlike *MUP-uPA* mice, it has been extremely difficult to detect the presence of such risk factors because they do not lead to overt liver damage (elevated ALT) prior to development of a steatotic liver due to hypernutrition. Given its presence in other pre-HCC conditions (Malhi and Kaufman, 2011), we focused our study on the role of ER stress. Remarkably, feeding a HFD to *MUP-uPA* mice resulted in steatohepatitis that closely resembled human NASH, and two of the main pathological features, ballooning degeneration and hepatocyte death, were also rapidly induced by the administration of tunicamycin to HFD-fed mice. By itself, short-term administration of tunicamycin did not damage the liver, but due to toxicity that may be associated with long-term use, we did not examine whether tunicamycin induces NASH and HCC in HFD-fed *WT* mice. Notably, NASH-like disease in *MUP-uPA* mice is associated with the same metabolic alterations linked

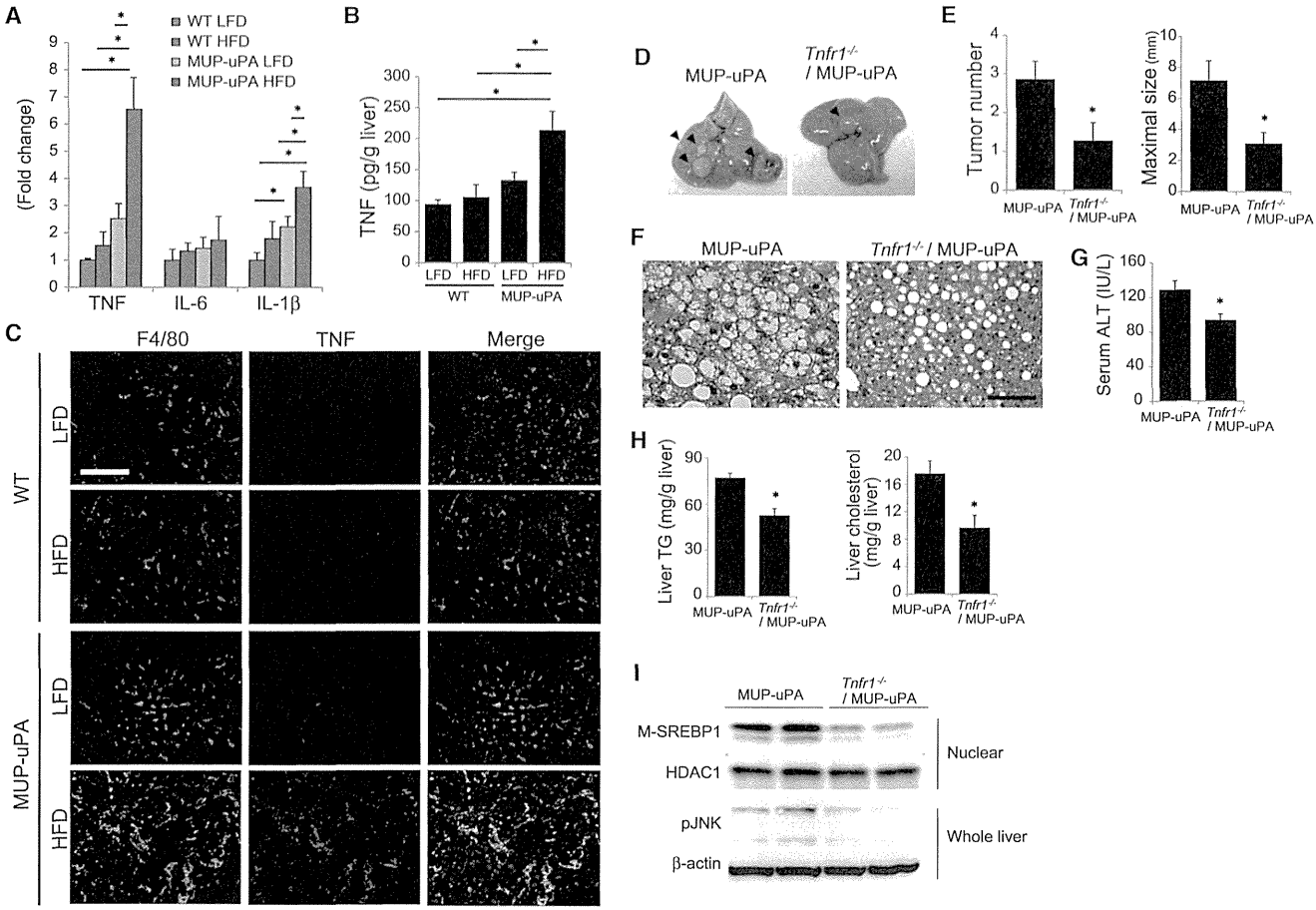

Figure 5. TNFR1 Signaling Promotes Tumor Growth

(A) Relative inflammatory cytokine mRNA in livers of 24-week-old mice kept on the LFD or HFD determined by real-time qPCR. Data are means ± SD (LFD-fed *WT*, n = 3; others, n = 5 per group). *p < 0.05.

(B) TNF protein in livers from (A) was measured using ELISA. Data are means ± SD. *p < 0.05.

(C) Double IF analysis of F4/80 (green) and TNF (red) of liver sections from (A) (scale bar, 100 μm). Nuclei were labeled with DAPI (blue).

(D–G) Effect of TNFR1 ablation on NASH and tumorigenesis in HFD-fed *MUP-uPA* mice. *MUP-uPA* and *Tnfr1*$^{-/-}$*/MUP-uPA* mice were fed the HFD from 6 to 40 weeks of age. Representative images of livers (D), tumor numbers and maximal sizes (E), H&E staining of nontumor areas (scale bar, 100 μm) (F), and serum ALT (G) are shown. Bar graphs represent means ± SEM (*MUP-uPA*, n = 14; *Tnfr1*$^{-/-}$*/MUP-uPA*, n = 11). *p < 0.05.

(H) TG and cholesterol content in nontumor tissue of HFD-fed *MUP-uPA* and *Tnfr1*$^{-/-}$*/MUP-uPA* mouse livers. Bar graphs represent means ± SD (n = 7 per group). *p < 0.05.

(I) IB analyses showing effects of TNFR1 ablation on SREBP1 maturation and JNK phosphorylation in nontumor tissue of HFD-fed *MUP-uPA* mice.

See also Figure S5.

to NASH in humans and is not accompanied by weight loss, as seen in other NASH models that are based on feeding mice toxic diets that induce liver damage (Farrell et al., 2012). Furthermore, the HFD-fed *MUP-uPA* mouse is currently the only model for studying obesity-induced HCC development that does not rely on the administration of liver toxins or carcinogens. The major NASH-promoting effects of ER stress in this system are increased lipogenesis, oxidative stress, and susceptibility to lipotoxic cell death. ER stress contributes to SREBP activation, thereby stimulating lipogenesis (Kammoun et al., 2009). ER and oxidative stress also upregulate several cell-death mediators, including TRB3 and DR5, but the exact mechanisms through which ER stress promotes cell death remain controversial (Xu et al., 2005) and our results indicate that in normal hepatocytes it is CHOP independent. Although ER stress causes insulin resistance (Hotamisligil, 2010; Ozcan et al., 2006) and insulin resistance was proposed to contribute to HCC development, our results suggest that insulin resistance has no obvious role in HCC development because it is not higher in *MUP-uPA* mice than in HFD-fed *WT* mice.

A consequence of ER stress and lipotoxic hepatocyte death that contributes to HCC development is induction of TNF-dependent steatohepatitis. In addition to amplifying liver inflammation and shaping the inflammatory microenvironment near HcPC clusters, TNF contributes to hepatosteatosis and liver damage. Although TNFR1 engagement can trigger apoptosis, it is not responsible for ER-stress-induced death in lean *MUP-uPA* mice, and its contribution to liver damage in HFD-fed mice is proportional to its effect on lipogenesis and may be indirect. TNF, however, directly stimulates HCC growth through NF-κB

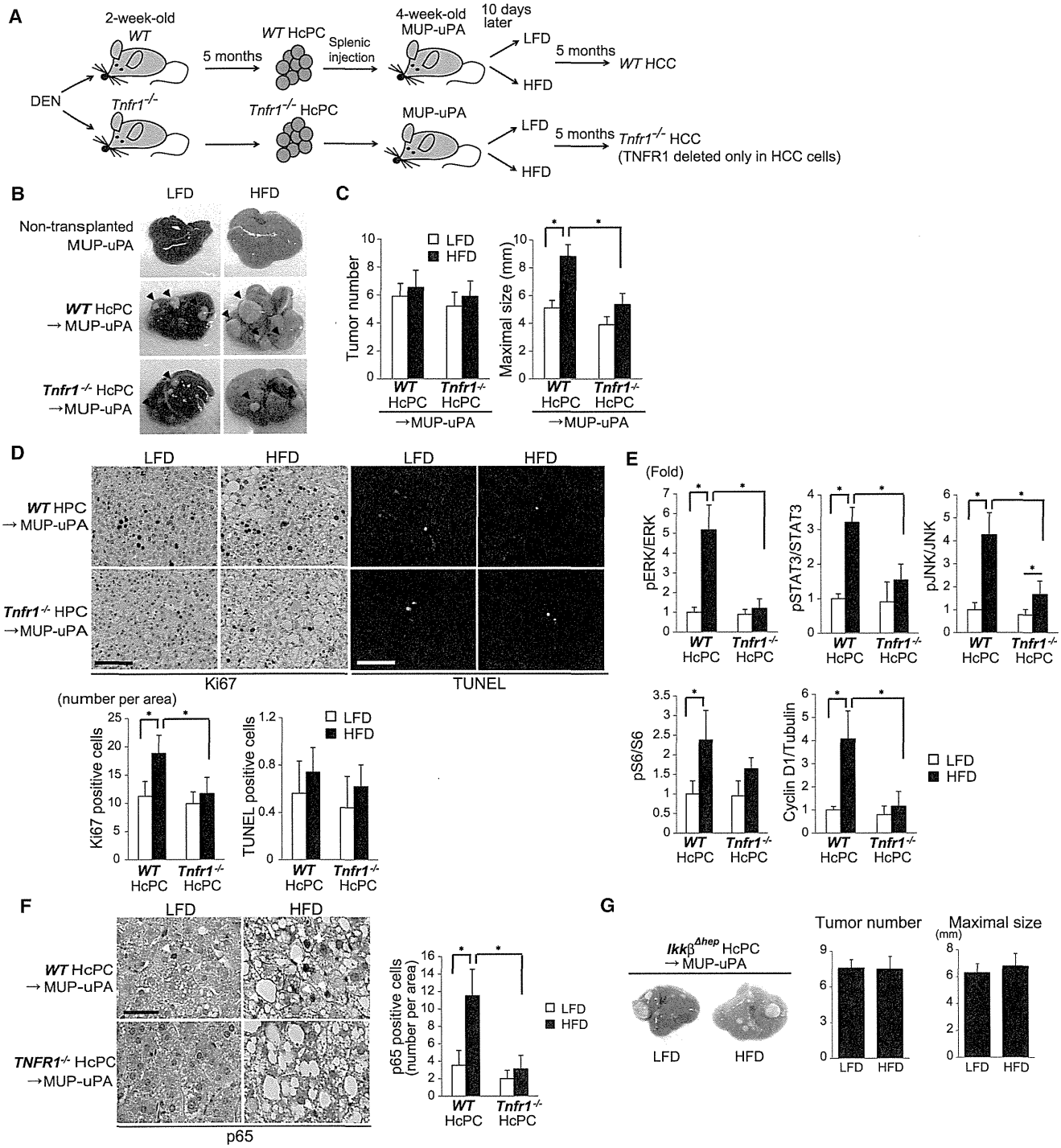

Figure 6. TNFR1 Signaling Promotes Tumor Growth

(A) HcPC isolation from DEN-treated *WT* and *Tnfr1*$^{-/-}$ mice and transplantation into *MUP-uPA* mice. HcPC-transplanted *MUP-uPA* mice were divided into two groups that were fed with either the LFD or HFD, and 5 months later tumorigenesis was assessed.

(B) Representative images of nontransplanted and HcPC-transplanted *MUP-uPA* mouse livers.

(C) Tumor numbers and maximal sizes. Results are means ± SEM (n = 10–11 per group). *p < 0.05.

(D) Ki67 IHC and TUNEL staining of tumor areas in livers in (C) (scale bar, 100 μm). Bars represent numbers of apoptotic and necrotic cells and Ki67-positive cells per field. Results are means ± SD (n = 6 per group). *p < 0.05.

(E) Tumor tissues from *WT* or *Tnfr1*$^{-/-}$ HcPC-transplanted *MUP-uPA* mice kept on the LFD or HFD were IB analyzed for phosphorylation of ERK, STAT3, JNK, and S6, and expression of cyclin D1. Data were quantified using Image J software and are presented as means ± SD (n = 5–6 per group). *p < 0.05.

(legend continued on next page)

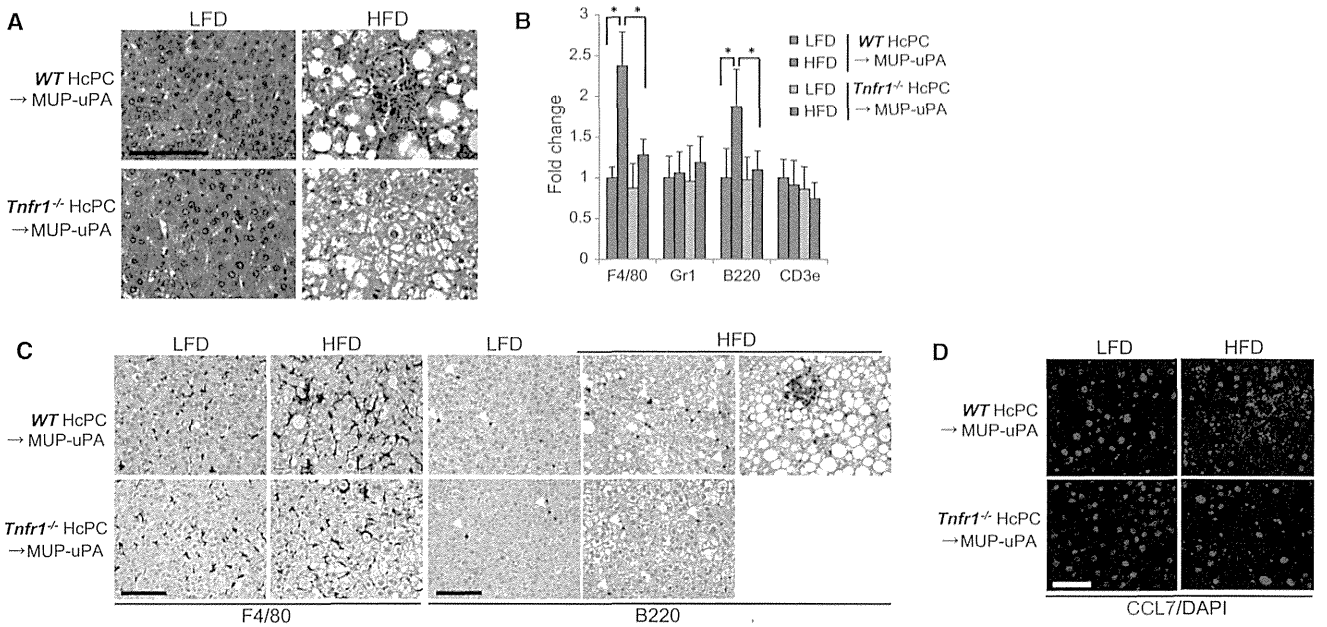

Figure 7. TNFR1 Signaling in Cancer Cells Promotes Tumor-Elicited Inflammation

(A) H&E analysis of tumors from *WT* or *Tnfr1*$^{-/-}$ HcPCs in *MUP-uPA* mice that were kept on the LFD or HFD (scale bar, 100 μm).

(B) Real-time PCR determination of immune cell marker mRNAs in tumor tissues. Data are means ± SD (n = 5 per group). *p < 0.05.

(C) IHC analysis of F4/80- and B220-positive cells in tumor tissues in (A) (scale bar, 100 μm).

(D) IF analysis of CCL7 expression in tumor tissues (scale bar, 25 μm).

See also Figure S7.

activation, but additional downstream TNFR1 effectors, such as JNK (Sakurai et al., 2008), may also contribute to HCC growth as well as hepatocyte death. TNF expression is also elevated in human NASH and anti-TNF therapy may reduce NASH activity (Schramm et al., 2008).

Although HFD feeding to *MUP-uPA* mice results in the upregulation of multiple cytokines and growth factors including several that stimulate HCC development, namely HGF and lymphotoxin (Haybaeck et al., 2009), anti-TNF therapy inhibited the obesity-enhanced progression of HcPCs to HCC and TNFR1 ablation almost completely blocked HCC development. We therefore suggest that anti-TNF drugs, perhaps in combination with improved intrahepatic delivery of chemical chaperons, such as TUDCA, should be evaluated for the inhibition of NASH-to-HCC progression and the treatment of steatohepatitic HCC along with more conventional chemotherapy.

EXPERIMENTAL PROCEDURES

Animals

MUP-uPA mice were kindly provided by E.P. Sandgren, University of Wisconsin-Madison (Weglarz et al., 2000). Liver-specific *Ikkβ*$^{\Delta hep}$ mice were described (Maeda et al., 2005). *Chop*$^{\Delta hep}$ mice were generated by crossing *Alb-Cre* mice with *Chop*$^{F/F}$ mice, which were developed by R.J.K together with Ira Tabas with the support of NIH grants DKD88227, DKD42394, and HLD52173. *Tnfr1*$^{-/-}$ mice were purchased from Jackson Laboratory (Bar Harbor). All animal studies were performed in accordance with NIH guidelines for the use and care of live animals and approved by University of California, San Diego (UCSD) Institutional Animal Care and Use Committee, S00218. All mouse lines were either on a pure C57BL/6 genetic background or crossed into it for at least ten generations. Studies were conducted on male mice maintained in filter-topped cages on autoclaved water and a regular chow diet (LFD, composed of 12% fat, 23% protein, and 65% carbohydrates based on caloric content) or a HFD (composed of 59% fat, 15% protein, and 26% carbohydrates based on caloric content; BioServ) according to UCSD and NIH guidelines.

HcPC Isolation and Transplantation

DEN (Sigma) was i.p. injected into male mice (25 mg/kg) on postnatal day 14. After 5 months, HcPCs were isolated as described and transplanted into 4-week-old *MUP-uPA* (He et al., 2013).

Primary Hepatocytes Cultures

Primary hepatocytes were isolated (He et al., 2013) and cultured in William's E medium with 10% fetal bovine serum (FBS) on collagen-coated plates. PA (Sigma) was dissolved in ethanol at 50°C and then diluted in BSA-containing RPMI-1640 medium that was applied to primary hepatocytes at a final concentration of 200 μM (to analyze signal transduction) or 300 μM (to analyze cell death).

(F) Activation of NF-κB analyzed by p65/RelA IHC in tumor tissues from *MUP-uPA* transplanted with *WT* or *Tnfr1*$^{-/-}$ HcPCs and kept on the LFD or HFD (scale bar, 25 μm). Bars show numbers of nuclear p65 positive cancer cells per 200× field. Data are means ± SD (n = 6 per group). *p < 0.05.

(G) Effect of IKKβ ablation on HFD-stimulated HcPC progression. HcPCs isolated from DEN-injected liver-specific *Ikkβ*$^{\Delta hep}$ were transplanted into *MUP-uPA* mice as in (A), and the HcPC-transplanted mice were kept on the LFD or HFD. After 5 months, tumor multiplicity and maximal sizes were determined. Data are means ± SEM (n = 10 per group).

See also Figure S6.

Hepatic Lipid Profile

Hepatic lipids were extracted using chloroform/methanol (2:1 v/v), and TG and total cholesterol contents were measured using Triglyceride Reagent Set (Pointe Scientific) and Cholesterol E (Wako), respectively. FA composition was analyzed using gas chromatography at SRL, Tokyo.

Biochemical Analyses and Reagents

Immunoblotting and real-time quantitative PCR (qPCR) were described (Maeda et al., 2005). Antibodies used were against phosphorylated ERK, ERK1/2, phosphorylated STAT3, STAT3, p-JNK, JNK1/2, phosphorylated S6, S6, p65, cyclinD1, and YAP (all from Cell Signaling); K19, GRP78, SREBP1, CHOP, CCL7, p62, and TNFR1 (all from Santa Cruz Biotechnology); p-eIF2α (Upstate); tubulin (Sigma); F4/80 (Molecular Probes); Ki67 (Gene Tex); AFP (Biocare Medical); TNF (R&D Systems); EpCAM (Abcam); and B220 (BD PharMingen). TUDCA and 4-PBA were from Calbiochem and Sigma, respectively. The GSH:GSSG ratio was analyzed using the GSSG/GSH Quantification Kit (Dojindo).

Histology

Livers were fixed in 10% neutral-buffered formalin or 4% paraformaldehyde, embedded in paraffin, sectioned, stained with hematoxylin and eosin (H&E) and Sirius Red, and processed for IHC. For frozen-block preparation, tissue was embedded in Tissue-Tek OCT compound (Sakura Finetek). IHC and IF analyses were described (He et al., 2013). Stained areas were quantitated using Image J software. Slides were incubated with primary antibodies, followed by secondary antibodies labeled with Alexa488 or Alexa594 (Molecular Probes). TUNEL staining was performed using an Apoalert DNA Fragmentation Assay kit (Clontech). Accumulation of superoxide anions was examined by DHE staining (Sakurai et al., 2008). Tissue sample preparation and EM analysis were described (Lee et al., 2012).

Infection of Recombinant Adenovirus

Primary hepatocytes were infected with recombinant adenovirus encoding β-galactosidase (LacZ) and GRP78 at a titer of 50 plaque-forming units/cell 4 hr after isolation.

Statistical Analyses

Statistical analyses were performed using student's t test or one-way ANOVA followed by the Tukey-Kramer test for multiple comparisons. The number of tumors larger than 2 mm was counted for comparative analyses of tumor development. A p value < 0.05 indicated statistical significance.

SUPPLEMENTAL INFORMATION

Supplemental Information includes seven figures and can be found with this article online at http://dx.doi.org/10.1016/j.ccr.2014.07.001.

AUTHOR CONTRIBUTIONS

H.N. designed and performed the main experiments, and wrote the paper. A.U. designed and performed the main experiments. K.T., J.F.-B., D.D., H.O., and Z.Z. provided technical assistance for the main experiments. E.S. and K.K. discussed and interpreted the results from the study. R.J.K. discussed and interpreted the results from the study, and provided a mouse line and reagents for the completion of the studies. J.H. provided a mouse line. M.A.V. made the pathological diagnosis and provided images of human steatohepatitic HCC. M.K. conceived, supervised, and wrote the paper.

ACKNOWLEDGMENTS

We thank Dr. E.P. Sandgren for *MUP-uPA*, Dr. I. Tabas for *Chop*$^{F/F}$ mice, and Dr. M.R. Mackey, Dr. G.A. Perkins, and Dr. M.H. Ellisman for help with the EM analysis. Research was supported by the Daiichi Sankyo Foundation of Life Science and Grant-in-Aid for Scientific Research (#25893042), and the Astellas Foundation for Research on Metabolic Disorders (H.N.); a Global Grant Scholarship from The Rotary Foundation (A.U.); a postdoctoral fellowship for Research Abroad, Research Fellowship for Young Scientists from the Japan Society for the Promotion of Science, and the Uehara Memorial Foundation Fellowship (K.T.); California Institute for Regenerative Medicine Stem Cell Training Grant II (TG2-01154; J.F.B.); the American Liver Foundation and a Young Investigator Award from the National Childhood Cancer Foundation "CureSearch" (D.D.); the Kanzawa Medical Research Foundation (H.O.); Cancer Research Institute Irvington Postdoctoral Fellowship (Z.Z.); grants from the NIH (CA155120-02 and CA118165-06; M.K.) and (DK042394-18, DK088227-06, and HL052173-16; R.J.K.), and Superfund Basic Research Program (P42ES010337; E.S. and M.K.). M.K. holds the Ben and Wanda Hildyard Chair for Mitochondrial and Metabolic Diseases and is an American Cancer Society Research Professor.

Received: January 2, 2014
Revised: May 28, 2014
Accepted: July 1, 2014
Published: August 14, 2014

REFERENCES

Anderson, E.J., Lustig, M.E., Boyle, K.E., Woodlief, T.L., Kane, D.A., Lin, C.T., Price, J.W., III, Kang, L., Rabinovitch, P.S., Szeto, H.H., et al. (2009). Mitochondrial H2O2 emission and cellular redox state link excess fat intake to insulin resistance in both rodents and humans. J. Clin. Invest. *119*, 573–581.

Brunt, E.M. (2001). Nonalcoholic steatohepatitis: definition and pathology. Semin. Liver Dis. *21*, 3–16.

Caldwell, S., Ikura, Y., Dias, D., Isomoto, K., Yabu, A., Moskaluk, C., Pramoonjago, P., Simmons, W., Scruggs, H., Rosenbaum, N., et al. (2010). Hepatocellular ballooning in NASH. J. Hepatol. *53*, 719–723.

Calle, E.E., Teras, L.R., and Thun, M.J. (2005). Obesity and mortality. N. Engl. J. Med. *353*, 2197–2199.

Chen, C.L., Yang, H.I., Yang, W.S., Liu, C.J., Chen, P.J., You, S.L., Wang, L.Y., Sun, C.A., Lu, S.N., Chen, D.S., and Chen, C.J. (2008). Metabolic factors and risk of hepatocellular carcinoma by chronic hepatitis B/C infection: a follow-up study in Taiwan. Gastroenterology *135*, 111–121.

Cohen, J.C., Horton, J.D., and Hobbs, H.H. (2011). Human fatty liver disease: old questions and new insights. Science *332*, 1519–1523.

Day, C.P., and James, O.F. (1998). Steatohepatitis: a tale of two "hits"? Gastroenterology *114*, 842–845.

DeZwaan-McCabe, D., Riordan, J.D., Arensdorf, A.M., Icardi, M.S., Dupuy, A.J., and Rutkowski, D.T. (2013). The stress-regulated transcription factor CHOP promotes hepatic inflammatory gene expression, fibrosis, and oncogenesis. PLoS Genet. *9*, e1003937.

El-Serag, H.B. (2011). Hepatocellular carcinoma. N. Engl. J. Med. *365*, 1118–1127.

Farrell, G.C., van Rooyen, D., Gan, L., and Chitturi, S. (2012). NASH is an inflammatory disorder: pathogenic, prognostic and therapeutic implications. Gut Liver *6*, 149–171.

Goldstein, J.L., DeBose-Boyd, R.A., and Brown, M.S. (2006). Protein sensors for membrane sterols. Cell *124*, 35–46.

Haybaeck, J., Zeller, N., Wolf, M.J., Weber, A., Wagner, U., Kurrer, M.O., Bremer, J., Iezzi, G., Graf, R., Clavien, P.A., et al. (2009). A lymphotoxin-driven pathway to hepatocellular carcinoma. Cancer Cell *16*, 295–308.

He, G., Dhar, D., Nakagawa, H., Font-Burgada, J., Ogata, H., Jiang, Y., Shalapour, S., Seki, E., Yost, S.E., Jepsen, K., et al. (2013). Identification of liver cancer progenitors whose malignant progression depends on autocrine IL-6 signaling. Cell *155*, 384–396.

Holzer, R.G., Park, E.J., Li, N., Tran, H., Chen, M., Choi, C., Solinas, G., and Karin, M. (2011). Saturated fatty acids induce c-Src clustering within membrane subdomains, leading to JNK activation. Cell *147*, 173–184.

Hotamisligil, G.S. (2010). Endoplasmic reticulum stress and the inflammatory basis of metabolic disease. Cell *140*, 900–917.

Inami, Y., Waguri, S., Sakamoto, A., Kouno, T., Nakada, K., Hino, O., Watanabe, S., Ando, J., Iwadate, M., Yamamoto, M., et al. (2011). Persistent activation of Nrf2 through p62 in hepatocellular carcinoma cells. J. Cell Biol. *193*, 275–284.